Aqueous Organometallic Chemistry of the Electrophilic $[(\eta\text{-}C_5(CH_3)_5)Ru(NO)]^{2+}$ Fragment

Anna Svetlanova-Larsen, Christopher R. Zoch, and John L. Hubbard*

Department of Chemistry and Biochemistry, Utah State University, Logan, Utah 84322-0300

Received April 2, 1996[⊗]

Treatment of Cp′Ru(NO)$(CH_3)_2$ with 2 equiv of $HOSO_2CF_3$ (HOTf) leads to the formation of the ditriflate complexes Cp′Ru(NO)$(OTf)_2$ (**1a,b**) (Cp′ = η-$C_5(CH_3)_5$, Cp* (**1a**), η-$C_5(CH_3)_4(CH_2CH_3)$, Cp† (**1b**)). The complex salts [Cp†Ru(NO)(OTf)(OH_2)][OTf] (**2b**) and [Cp†Ru(NO)$(OH_2)_2$][OTf]$_2$ (**3b**) can be isolated from the hydration of **1b**. The structures of **1b**, **2b**, and **3b** are determined by single-crystal X-ray diffraction methods. In 0.1 M H_2O/CH_2Cl_2 the equilibria **1a** $\overset{K_1}{\rightleftharpoons}$ **2a**$^+$ + OTf$^-$ $\overset{K_2}{\rightleftharpoons}$ **3a**$^{2+}$ + 2OTf$^-$ exist, with **1a** being the predominant complex and $\Delta H_1 = -15(3)$ kcal/mol and $\Delta S_1 = -60(30)$ eu (for K_1) and $\Delta H_2 = -9(1)$ kcal/mol and $\Delta S_2 = -40(25)$ eu (for K_2). For comparison, the equilibria **1a** $\overset{K_1}{\rightleftharpoons}$ [Cp*Ru(NO)(OTf)(THF)]$^+$ + OTf$^-$ $\overset{K_2}{\rightleftharpoons}$ [Cp*Ru(NO)$(THF)_2$]$^{2+}$ + 2OTf$^-$ exist in neat THF with $\Delta H_1 = -4.5(3)$ kcal/mol and $\Delta S_1 = -30(10)$ eu (for K_1) and $\Delta H_2 = -4.1(1)$ kcal/mol and $\Delta S_2 = -20(10)$ eu (for K_2). The anion exchange equilibria in CH_2Cl_2 **1a** + 2Cl$^-$ $\overset{K_1}{\rightleftharpoons}$ [Cp*Ru(NO)(OTf)(Cl) + OTf$^-$ + Cl$^-$ $\overset{K_2}{\rightleftharpoons}$ [Cp*Ru(NO)Cl_2] + 2OTf$^-$ has $\Delta H_1 = -9(1)$ kcal/mol and $\Delta S_1 = -30(10)$ eu (for K_1) and $\Delta H_2 = -11(1)$ kcal/mol and $\Delta S_2 = -30(10)$ eu (for K_2). While loss of the OTf$^-$ ligands is exothermic, the displacement of OTf$^-$ from the coordination sphere carries a significant entropy cost due to the formation of ions in a more-ordered solvent cage. Complex salts **1a,b** dissolve in water to give acidic red-orange solutions containing an equilibrium mixture of the diaqua complex cations [Cp′Ru(NO)$(OH_2)_2$]$^{2+}$ (**3a**$^{2+}$, pK_a = 2.7; **3b**$^{2+}$) and the dinuclear cations [Cp′Ru(NO)(μ-OH)]$_2^{2+}$ (**4a**$^{2+}$, pK_a = 5.5; **4b**$^{2+}$). The cations **4a**$^{2+}$ and **4b**$^{2+}$ exist as a mixture of *cis* (major) and *trans* (minor) isomers; X-ray results show **4b**$^{2+}$ to be *cis* in the solid state. Crossover between **4a**$^{2+}$ and **4b**$^{2+}$ to give the mixed Cp*/Cp† dimer **4c**$^{2+}$ occurs readily under acidic conditions but not under basic conditions. The pH dependence together with kinetic and van't Hoff analyses support the process 2 **3a**$^{2+}$ ⇄ **4a**$^{2+}$ + 2H_3O^+. The ∠Ru−N−O values of ca. 160°, correspondingly low ν_{NO} values in the Nujol mull IR spectra, and relatively short Ru−O bonds show the H_2O and OH$^-$ ligands to be significant π-donors to the electrophilic Ru center. Dissolution of **4a,b** in basic D_2O causes complete deuteration of the ring CH_3 groups but no deuteration of the Cp†-CH_2CH_3 group; the CD_3 groups are easily exchanged to CH_3 by exposure to basic H_2O conditions. Chloride substitution by H_2O occurs when Cp′Ru(NO)Cl_2 is dissolved in water, giving an equilibrium mixture of undissociated [Cp′Ru(NO)Cl_2]$_{aq}$ together with the [Cp′Ru(NO)(Cl)(OH_2)]$^+$ and [Cp′Ru(NO)(μ-OH)]$_2^{2+}$ ions. H/D exchange on the Cp′ ring CH_3 groups also occurs slowly when Cp′Ru(NO)Cl_2 is dissolved in D_2O but not when dissolved in a D_2O/DCl mixture. The present work suggests that Cp′-ring slippage and the reversible release of H^+/D^+ is facilitated by the π-donor ability of the H_2O and OH$^-$ ligands.

Introduction

Electrophilic transition metal complexes are an important part of modern catalysis.[1] Especially important in this area is the subject of metal−triflate (M−OTf) complexes that have seen increasing application as precursors to unsaturated electrophilic metal centers (OTf = OSO_2CF_3).[2] Such catalysts have been shown to accelerate Diels−Alder reactions by as much as 10^5 as compared to uncatalyzed reactions.[3] Dissociation of OTf$^-$ from chiral precursors leads to stereoselective

⊗ Abstract published in *Advance ACS Abstracts,* June 1, 1996.

(1) (a) Hlatky, G. G.; Turner, H. W.; Eckman, R. R. *J. Am. Chem. Soc.* **1989**, *111*, 2728. (b) Hlatky, G. G.; Eckman, R. R.; Turner, H. W. *Organometallics* **1992**, *11*, 1413. (c) Sishta, C.; Hawthorn, R. M.; Marks, T. J. *J. Am. Chem. Soc.* **1992**, *114*, 1112. (d) Marks, T. J. *Acc. Chem. Res.* **1992**, *23*, 57. (e) Yang, X.; Stern, C. L.; Marks, T. J. *J. Am. Chem. Soc.* **1991**, *113*, 3623. (f) Yang, X.; Stern, C. L.; Marks, T. J. *Organometallics* **1991**, *10*, 840. (g) Lin, Z.; Le Marechal, J.-F.; Sabat, M.; Marks, T. J. *J. Am. Chem. Soc.* **1987**, *109*, 4127. (h) Dalton, D. M.; Gladysz, J. A. *J. Organomet. Chem.* **1989**, *370*, C17. (i) Saura-Llamas, I.; Gladysz, J. A. *J. Am. Chem. Soc.* **1992**, *114*, 2136. (j) Klein, D. P.; Gladysz, J. A. *J. Am. Chem. Soc.* **1992**, *114*, 8710. (k) Winter, C. H.; Zhou, X.-X.; Heeg, M. J. *Inorg. Chem.* **1992**, *31*, 1808.

(2) (a) Lawrance, G. A. *Chem. Rev.* **1986**, *86*, 17. (b) Humphrey, R. B.; Lamanna, W. M.; Brookhart, M.; Husk, G. R. *Inorg. Chem.* **1983**, *22*, 3355. (c) Stang, P. J.; Huang, Y. H.; Arif, A. M. *Organometallics* **1992**, *11*, 231. (d) Stang, P. J.; Cao, D. H.; Poulter, G. T.; Arif, A. M. *Organometallics* **1995**, *14*, 1110. (e) Bennet, B. L.; Birnbaum, J.; Roddick, D. M. *Polyhedron* **1995**, *14*, 187. (f) Blosser, P. W.; Gallucci, J. C.; Wojcicki, A. *Inorg. Chem.* **1992**, *31*, 2376. (g) Beck, W.; Sünkel, K.; *Chem. Rev.* **1988**, *88*, 1405.

(3) (a) Hollis, T. K.; Robinson, N. P.; Bosnich, B. *Organometallics* **1992**, *11*, 2645. (b) Hollis, T. K.; Robinson, N. P.; Bosnich, B. *J. Am. Chem. Soc.* **1992**, *114*, 5464. (c) Bonnesen, P. V.; Puckett, C. L.; Honeychuck, R. V.; Hersh, W. H. *J. Am. Chem. Soc.* **1989**, *111*, 6070. (d) Honeychuck, R. V.; Bonnesen, P. V.; Farahi, J.; Hersh, W. H. *J. Org. Chem.* **1987**, *52*, 5293. Odenkirk, W.; Rheingold, A. L.; Bosnich, B. *J. Am. Chem. Soc.* **1992**, *114*, 6392.

S0276-7333(96)00257-9 CCC: $12.00

electrophilic metal catalysts.[4,5] There are several recent reports on the generation and reactivity of late-metal systems where triflate dissociation leads to catalysts that copolymerize CO and olefins.[6] Triflate dissociation from (η^3-1,4,7-trimethyl-1,4,7-triazacyclononane)Rh-$(CH_3)(OTf)_2$ and related species has been shown to initiate ethylene polymerization even in the presence of water.[7] The study of aqueous organometallic chemistry has a long history dating back into the 1800's and has reemerged as an important area of study because of the environmentally and financially benevolent properties of water-based processes.[8] Synthetic reactions performed in aqueous media can actually exhibit higher activity and better selectivity than in organic solvents.[7,9,10] Furthermore, there is an increasing demand to study catalysis that is more closely related to the chemistry in naturally-occurring biocatalytic systems.

Continuing from our interest in complexes containing the versatile [Cp′Ru(NO)] fragment,[11,12] we present here the characterization of the Lewis acid nature of the $[Cp'Ru(NO)]^{2+}$ fragment (Cp′ = η-$C_5(CH_3)_5$, Cp*, and η-$C_5(CH_3)_4(CH_2CH_3)$, Cp†). Previous work from Brookhart and from our laboratory shows that the $[Cp^*Ru(NO)(R)]^+$ fragment, generated by H_2O dissociation from $[Cp^*Ru(NO)(CH_3)(H_2O)]^+$ or by OTf^- dissociation from $Cp^*Ru(NO)(CH_3)(OTf)$, can bind and activate olefins[13] and alkynes.[11] While some kinetic aspects of OTf^- substitution have been described,[14] a comprehensive characterization of the equilibrium between bound and free OTf^- in the presence of coordinating solvents has yet to be reported.[15] In particular, it is important to distinguish between the materials that crystallize from a solution and the actual species *present* in solution.

The systems we present here offer a simple format for the evaluation of H_2O and OTf^- as a competing ligands in the presence of an electrophilic metal center. Although water is considered a common ligand in coordination chemistry,[16] there is still considerable interest in the nature of water and hydroxo ligands in organometallic systems, especially in regard to their ability to displace coordinating counterions and reactive substrates.[17] We show the ancillary NO ligand to be especially valuable because the ν_{NO} and $\angle$Ru−N−O values provide insight about the π-donor ability of the H_2O ligand.[18] The work here employs a combination of traditional techniques like pH, conductivity measurements, and structural methods coupled with a direct assessment of chemical equilibria and kinetics by NMR spectroscopy in H_2O.

Results

Synthesis and Characterization of Complexes 1a,b. Treatment of CH_2Cl_2 solutions of Cp′Ru(NO)-$(CH_3)_2$ with slightly more than 2 equiv of HOTf results in a color change from red to purple, the evolution of CH_4, and the quantitative formation of the Cp*Ru(NO)-$(OTf)_2$ (**1a**) or $Cp^\dagger Ru(NO)(OTf)_2$ (**1b**) as determined by ^{1}H NMR spectroscopy. Intermediate in the formation of **1a,b** are the Cp′Ru(NO)(CH_3)(OTf) complexes.[11] The ^{1}H NMR spectra of CH_2Cl_2 solutions of **1a,b** show a single Cp′ environment and the ^{19}F NMR spectra of these solutions exhibit a single resonance at δ −77.0.

(4) Jaquith, J. B.; Guan, J.; Wang, S.; Collins, S. *Organometallics* **1995**, *14*, 1079.
(5) Saura-Llamas, I.; Garner, C. M.; Gladysz, J. A. *Organometallics* **1991**, *10*, 2533.
(6) (a) Rix, F. C.; Brookhart, M. *J. Am. Chem. Soc.* **1995**, *117*, 1137. (b) Johnson, L. K.; Killian, C. M.; Brookhart, M. *J. Am. Chem. Soc.* **1995**, *117*, 6414.
(7) (a) Wang, L.; Flood, T. C. *J. Am. Chem. Soc.* **1992**, *114*, 3169. (b) Wang, C.; Ziller, J. W.; Flood, T. C. *J. Am. Chem. Soc.* **1995**, *117*, 1647. (c) Wang, L.; Lu, R. S.; Bau, R.; Flood, T. C. *J. Am. Chem. Soc.* **1993**, *115*, 6999.
(8) *Principles of Organotransition Metal Chemistry*; Collman, J. P., Hegedus, L. S., Norton, J. R., Finke, R. G., Eds.; University Science Books: Mill Valley, CA, 1987; Chapter 1 and references therein.
(9) (a) Haggin, J. *Aqueous media Offer Promises And Problems In Organometallic Catalysis. Chem. Eng. News* **1994**, Oct 10, 28−33. (b) Fish, R. H.; Baralt, E.; Kim, H.-S. *Organometallics* **1991**, *10*, 1965. (c) Baralt, E.; Smith, S. J.; Hurwitz, J.; Horvath, I. T.; Fish, R. H. *J. Am. Chem. Soc.* **1992**, *114*, 5187. (d) Smith, D. P.; Baralt, E.; Moreles, B.; Olmstead, M. M.; Maestre, M. F.; Fish, R. H. *J. Am. Chem. Soc.* **1992**, *114*, 10647. (e) Smith, D. P.; Olmstead, M. M.; Noll, B. C.; Maestre, M. F.; Fish, R. F. *Organometallics* **1993**, *12*, 593. (f) Smith, D. P.; Griffin, M. T.; Olmstead, M. M.; Maestre, M. F.; Fish, R. H. *Inorg. Chem.* **1993**, *32*, 4677. (g) Chen, H.; Maestre, M. F.; Fish, R. H. *J. Am. Chem. Soc.* **1995**, *117*, 3631. (h) Eisen, M. S.; Haskel, A.; Chen, H.; Olmstead, M. M.; Smith, D. P.; Maestre, M. F.; Fish, R. H. *Organometallics* **1995**, *14*, 2806. (i) Karlen, T.; Ludi, A. *J. Am. Chem. Soc.* **1994**, *116*, 11375. (j) McGrath, D. V.; Grubbs, R. H. *Organometallics* **1994**, *13*, 224. (k) Dadci, L.; Elias, H.; Frey, U.; Hörnig, A.; Koelle, U.; Merbach, A. C.; Paulus, H.; Schneider, J. S. *Inorg. Chem.* **1995**, *34*, 306−315. (l) Darensbourg, D. J.; Joo, F.; Kannisto, M.; Katho, A.; Reibenspies, J. H.; Daigle, D. J. *Inorg. Chem.* **1994**, *33*, 200. (m) Darensbourg, D. J.; Stafford, N. W.; Joo, F.; Reibenspies, J. H. *J. Organomet. Chem.* **1995**, *488*, 99. (n) Barton, M.; Atwood, J. D. *J. Coord. Chem.* **1991**, *24*, 43−67. (o) Rauscher, D. J.; Thaler, E. G.; Huffman, J. C.; Caulton, K. G. *Organometallics* **1991**, *10*, 2209. (p) Labinger, J. A.; Herring, A. M.; Lyon, D. K.; Luinstra, G. A.; Bercaw, J. E.; Horvath, I. T.; Eller, K. *Organometallics* **1993**, *12*, 895. (q) Agbossou, S. K.; Roger, C.; Igau, A.; Gladysz, J. A. *Inorg. Chem.* **1992**, *31*, 419. (r) Le, T. X.; Merola, J. S. *Organometallics* **1993**, *12*, 3798. (s) Herrmann, W. A.; Kohlpaintner, C. W. *Angew. Chem., Int. Ed. Engl.* **1993**, *32*, 1524−1544. (t) Dobbs, D. A.; Bergman, R. G. *Organometallics* **1994**, *13*, 4594. (u) Bartik, T.; Bartik, B.; Hanson, B. E.; Guo, I.; Toth, I. *Organometallics* **1993**, *12*, 164. (v) Mandel, S. K.; Chakravarty, A. R. *Inorg. Chem.* **1993**, *32*, 3851. (w) Legzdins, P.; Lundmark, P. J.; Phillips, E. C.; Rettig, S. J.; Veltheer, J. E. *Organometallics* **1992**, *11*, 2991.
(10) (a) Kang, J. W.; Maitlis, P. M. *J. Organomet. Chem.* **1971**, *30* (1), 127. (b) Nutton, A.; Bailey, P.; Maitlis, P. M. *J. Chem. Soc., Dalton Trans.* **1981**, 1997. (c) Hirai, K.; Nutton, A.; Maitlis, P. M. *J. Mol. Catal.* **1981**, *203−211*, 203. (d) Nutton, A.; Maitlis, P. M. *J. Chem. Soc., Dalton Trans.* **1981**, 2335. (e) Miguel-Garcia, J. A.; Adams, H.; Bailey, N. A.; Maitlis, P. M. *J. Organomet. Chem.* **1991**, *413*, 427. (f) Gusev, O. V.; Rubezhov, A. Z.; Miguel-Garcia, J. A.; Maitlis, P. M. *Mendeleev Commun.* **1991**, 21. (g) Wei, C.; Aigbirhio, F.; Adams, H.; Bailey, N. A.; Hempstead, P. D.; Maitlis, P. M. *J. Chem. Soc., Chem. Commun.* **1991**, 883. (h) Miguel-Garcia, J. A.; Adams, H.; Bailey, N. A.; Maitlis, P. M. *J. Chem. Soc., Dalton Trans.* **1992**, 131. (i) Gusev, O.; Sergeev, S.; Saez, I. M.; Maitlis, P. M.; *Organometallics* **1994**, *13*, 2059. (j) Fan, L.; Turner, M. L.; Hursthouse, M. B.; Abdul Malik, K. M.; Gusev, O. V.; Maitlis, P. M. *J. Am. Chem. Soc.* **1994**, *116*, 385.
(11) Hubbard, J. L.; Burns, R. M. *J. Am. Chem. Soc.* **1994**, *116*, 9514.
(12) (a) Hubbard, J. L.; Morneau, A.; Burns, R. M.; Zoch, C. R. *J. Am. Chem. Soc.* **1991**, *113*, 9176. (b) Hubbard, J. L.; Morneau, A.; Burns, R. M.; Nadeau, O. W. *J. Am. Chem. Soc.* **1991**, *113*, 9180.
(13) Hauptman, E.; Brookhart, M.; Fagan, P. J.; Calabrese, J. C. *Organometallics* **1994**, *13*, 774.
(14) (a) Nitschke, J.; Schmidt, S. P.; Trogler, W. C. *Inorg. Chem.* **1985**, *24*, 1972. (b) Trogler, W. C. *J. Am. Chem. Soc.* **1979**, *101*, 6459.
(15) Hoffman and co-workers have reported the ranges for the equilibrium constants for square planar Rh^IOTf^- complexes: (a) Branan, D. M.; Hoffman, N. W.; McElroy, E. A.; Prokopuk, N.; Salazar, A. B.; Robbins, M. J.; Hill, W. E.; Webb, T. R. *Inorg. Chem.* **1991**, *30*, 1200. (b) Branan, D. M.; Hoffman, N. W.; McElroy, E. A.; Ramage, D. L.; Robbins, M. J.; Eyler, J. R.; Watson, C. H.; deFur, P.; Leary, J. A *Inorg. Chem.* **1990**, *29*, 1915. (c) Araghizadeh, F.; Branan, D. M.; Hoffman, N. W.; Jones, J. H.; McElroy, E. A.; Miller, N. C.; Ramage, D. L.; Salazar, A. B.; Young, S. H. *Inorg. Chem.* **1988**, *27*, 3752.
(16) (a) Grover, N.; Gupta, N.; Thorp, H. H. *J. Am. Chem. Soc.* **1992**, *114*, 3390. (b) Call, J. T.; Hughes, K. A.; Harman, W. D.; Finn, M. G. *Inorg. Chem.* **1993**, *32*, 2123. (c) Banyai, I.; Glaser, J.; Read, M. C.; Sandstrom, M. *Inorg. Chem.* **1995**, *34*, 2423. (d) Dimitrou, K.; Folting, K.; Streib, W. E.; Christou, G. *J. Am. Chem. Soc.* **1993**, *115*, 6432.
(17) (a) Lou, X.-L.; Schulte, G. K.; Crabtree, R. H. *Inorg. Chem.* **1990**, *29*, 682. (b) Kubas, G. J.; Burns, C. J.; Khalsa, G. R. K.; Van Der Sluys, L. S.; Kiss, G.; Hoff, C. D. *Organometallics* **1992**, *11*, 3390.
(18) For comparison, the π-donor abilities of halide ligands are now recognized as being very important for stabilizing coordinatively unsaturated metal centers: (a) Rothfuss, H.; Huffman, J. C.; Caulton, K. G. *J. Am. Chem. Soc.* **1994**, *116*, 187. (b) Gusev, D. G.; Kulhman, R.; Rambo, J. R.; Berke, H.; Eisenstein, O.; Caulton, K. G. *J. Am. Chem. Soc.* **1995**, *117*, 281. (c) Johnson, T. J.; Folting, K.; Streib, W. E.; Martin, J. D.; Huffman, J. C.; Jackson, S. A.; Eisenstein, O.; Caulton, K. G. *Inorg. Chem.* **1995**, *34*, 488. (d) Caulton, K. G. *New J. Chem.* **1994**, *18*, 25.

Table 1. Summary of Crystallographic Data for Complexes 1b, 2b, 3b, and 4b

	1b	2b	3b	4b
formula	$C_{13}H_{17}NO_7S_2F_6Ru$	$C_{13}H_{19}NO_8S_2F_6Ru$	$C_{13}H_{21}NO_9F_6S_2Ru$	$C_{24}H_{36}N_2O_{10}F_6S_2Ru_2$
fw	578.5	596.5	614.5	446.1
cryst system	monoclinic	triclinic	monoclinic	orthorhombic
space group	$P2_1/n$ (No. 14)	$P\bar{1}$ (No. 2)	$C2/m$ (No. 12)	$Pbcn$ (No. 60)
a (Å)	8.657(2)	8.431(4)	21.380(4)	15.148(4)
b (Å)	9.503(2)	8.571(4)	8.907(2)	14.809(3)
c (Å)	26.388(5)	14.893(9)	13.481(3)	15.214(6)
α (deg)	90	93.44(4)	90	90
β (deg)	97.11(2)	91.94(4)	115.70(3)	90
γ (deg)	90	92.75(4)	90	90
V (Å^3)	2154.3(7)	1072.3(9)	2113.2(8)	3410.0(6)
Z	4	2	4	4
T (K)	298	173	223	173
μ(Mo Kα) (mm^{-1})	1.006	1.02	0.95	1.09
ρ_{calc} (g/cm^3)	1.784	1.847	1.76	1.74
final R, R_w	0.0496,[a] 0.0631[b]	0.0297,[a] 0.0382[b]	0.0569,[a] wR_2 = 0.1536[c]	0.0309,[a] 0.0432[b]

[a] $R = \sum||F_o| - |F_c||/\sum|F_o|$. [b] $R_w = [\sum w(|F_o| - |F_c|)^2/\sum w|F_o|^2]^{1/2}$; $w = 1/\sigma^2(|F_o|)$. [c] w$R2 = |\sum[w(F_o^2 - F_c^2)]^2]/\sum[w(F_o^2)^2]]^{1/2}$.

Table 2. Selected Geometric Data for 1b[a]

Bond Lengths (Å)			
Ru−N	1.772(8)	S(2)−C(7)	1.745(17)
Ru−O(2)	2.133(5)	S(2)−O(5)	1.461(6)
Ru−O(5)	2.125(5)	S(2)−O(6)	1.456(10)
N−O(1)	1.136(11)	S(2)−O(7)	1.344(9)
S(1)−C(6)	1.812(19)	C−F$_{av}$	1.31(2)
S(1)−O(2)	1.473(5)	Cp$^{\dagger}_{cent}$−Ru	1.85
S(1)−O(3)	1.381(7)	O(4)---C(11)	3.25
S(1)−O(4)	1.430(9)	O(6)---C(14)	3.26

Bond Angles (deg)			
N−Ru−O(2)	102.9(3)	Ru−O(5)−S(2)	129.8(3)
N−Ru−O(5)	102.0(3)	O(5)−Ru−O(2)	79.8(2)
O(2)−Ru−O(5)	79.8(2)	N−Ru−O2	102.9(3)
Ru−N−O(1)	164.2(7)	N−Ru−O(5)	102.0(3)
Ru−O(2)−S(1)	128.9(3)		

[a] Cp$^{\dagger}_{cent}$ = centroid of η-$C_5(CH_3)_4(CH_2CH_3)$ ligand.

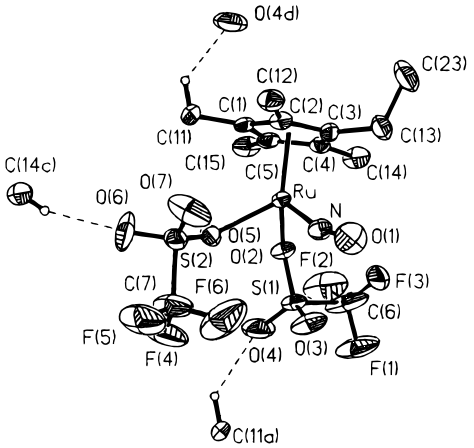

Figure 1. Thermal ellipsoid plot (30% probability level) and atom-numbering scheme for **1b**. Dashed lines indicate closest contacts in the extended lattice (see Table 2).

The IR spectra for **1a,b** in CH_2Cl_2 show characteristic ν_{NO} values at 1848 and 1851 cm^{-1}, respectively. The electronic absorption spectra of **1a,b** in CH_2Cl_2 show maxima at 378 and 556 nm. Complexes **1a,b** precipitate from CH_2Cl_2 by the addition of Et_2O to give thermally stable bluish-purple solids that are unreactive with O_2 but are best stored under N_2 in order to avoid rapid reaction with atmospheric water (*vide infra*).

The characterization of complex **1b** by single-crystal X-ray analysis is summarized in Tables 1 and 2. Figure 1 shows the molecule to possess a three-legged piano stool geometry with the OTf$^-$ ions O-bound to the metal with an average Ru−O bond distance of 2.129(7) Å. The Ru−N−O(1) bond angle is 164.2(7)°, and the O(2)−Ru−O(5) bond angle is 79.8(2)°. The O(4) atom of one OTf$^-$ ligand is 3.25 Å from the C(11) methyl carbon of a neighboring complex. The O(6) atom of the other OTf$^-$ ligand is 3.26 Å from the C(14) methyl carbon of another neighboring complex, giving rise to an extended weak H-bonding array in the solid-state. The CF_3 groups have an average C−F distance of 1.31 Å and do not make any close contacts with any other atoms.

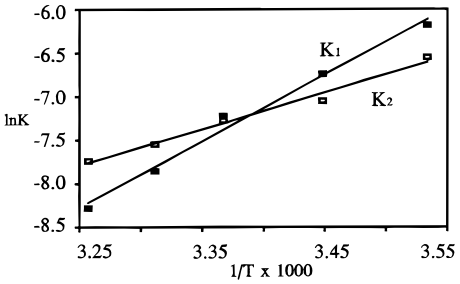

Figure 2. van't Hoff plots for the equilibrium of complex **1a** with H_2O in CH_2Cl_2.

Substitution of OTf$^-$ in Organic Solvents. Dissolution of **1a** in 0.1 M H_2O/CH_2Cl_2 gives a purple solution that displays three signals in the ^{19}F NMR spectrum. The major resonance at δ −77.0 is identified as Cp*Ru(NO(OTf)$_2$, and two minor broad resonances at δ −76.7 and δ −78.6 are assigned as the monoaqua $[Cp^*Ru(NO)(OTf)(OH_2)]^+$ cation (**2a**$^{2+}$) and free OTf$^-$, respectively. The intensity due to free OTf$^-$ is greater than the intensity of the signal from **2a**$^+$ inferring the presence of a third (and ^{19}F NMR silent) cationic complex $[Cp^*Ru(NO)(OH_2)_2]^{2+}$ (**3a**$^{2+}$). The amount of **3a**$^{2+}$ is readily determined from the initial concentration of **1a** and the measured integrals of **2a**$^+$ and free OTf$^-$ versus an internal standard (see Experimental Section). The ^{19}F NMR signal intensities are temperature dependent, and the results of a van't Hoff analysis for the two-step equilibrium process of eq 1 are shown in Figure

$$\mathbf{1a} \underset{0.1\text{ M } H_2O/CH_2Cl_2}{\overset{K_1}{\rightleftharpoons}} \underset{\mathbf{2a}^+}{[Cp^*Ru(NO)(OTf)(OH_2)]^+} + OTf^- \underset{0.1\text{M } H_2O/CH_2Cl_2}{\overset{K_2}{\rightleftharpoons}} \underset{\mathbf{3a}^{2+}}{[Cp^*Ru(NO)(OH_2)_2]^{2+}} + 2OTf^- \quad (1)$$

2, giving $\Delta H_1 = -15(3)$ kcal/mol and $\Delta S_1 = -60(30)$ eu for K_1 and $\Delta H_2 = -8(1)$ kcal/mol and $\Delta S_2 = -40(20)$ eu for K_2. At 298 K, the solution contains a ca. 20:5:1 mixture of **1a**, **2a**$^+$, and **3a**$^{2+}$, respectively. The errors in ΔS are large due to the restriction of the analysis to

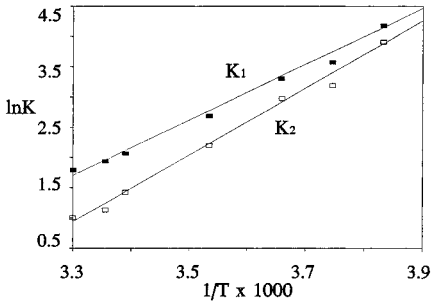

Figure 3. van't Hoff plots for the equilibrium of complex **1a** with Cl^- in CH_2Cl_2.

a relatively small temperature range (between +10 and +35 °C) to avoid the separation of an aqueous phase at lower temperatures. If 10 equiv of HOTf is added to the solution, OTf^- dissociation from **1a** is completely suppressed.

As monitored by ^{19}F NMR spectroscopy, the addition of 2 equiv of $[Ph_3PNPPh_3]Cl$ to **1a** dissolved in dry CH_2Cl_2 results in the decrease of the original δ −77.0 signal and the appearance of new signals at δ −77.2 assigned as Cp*Ru(NO)(OTf)(Cl) and free OTf^- at δ −78.6. The intensity due to free OTf^- is greater than the intensity of the signal from Cp*Ru(NO)(OTf)(Cl), inferring the presence of a third (and ^{19}F NMR silent) complex Cp*Ru(NO)Cl_2. The ^1H NMR spectrum of this mixture indeed shows a signal for Cp*Ru(NO)Cl_2 at δ 1.84 and a signal at δ 1.82 assigned to Cp*Ru(NO)(OTf)(Cl) in addition to the original δ 1.88 signal of Cp*Ru(NO)-$(OTf)_2$. Quantitation of Cp*Ru(NO)Cl_2 by ^{19}F NMR spectroscopy is based on the initial concentration of **1a** and measuring the integral intensities of Cp*Ru(NO)-(OTf)Cl and free OTf^- versus an internal standard (see Experimental Section). The NMR spectra are temperature dependent, and the results of a van't Hoff analysis for the two-step equilibrium process (eq 2) give $\Delta H_1 = 9(1)$ kcal/mol and $\Delta S_1 = -30(10)$ eu for K_1 and $\Delta H_2 = 11(1)$ kcal/mol and $\Delta S_2 = -30(10)$ eu for K_2 (Figure 3). At 298 K, the solution contains a ca. 1:2:7 mixture of **1a**, Cp*Ru(NO(OTf)(Cl), and Cp*Ru(NO)Cl_2, respectively. Dissolution of **1a** in neat THF gives red solutions

$$\mathbf{1a} + 2Cl^- \overset{K_1}{\rightleftharpoons} [Cp^*Ru(NO)(OTf)Cl] + OTf^- + Cl^- \overset{K_2}{\rightleftharpoons} Cp^*Ru(NO)Cl_2 + 2OTf^- \quad (2)$$

(λ_{max} = 536 nm) with an ^{19}F NMR signal of free OTf^- at δ −78.7 and two other signals at δ −77.4 and −77.0 assigned as the Cp*Ru(NO)$(OTf)_2$ and $[Cp^*Ru(NO)(OTf)(THF)]^+$ complexes, respectively, on the basis of their intensities relative to that of free OTf^-. The quantity of the ^{19}F NMR-silent species $[Cp^*Ru(NO)(THF)_2]^{2+}$ is deduced from the amount of free OTf^- not accounted to the formation of $[Cp^*Ru(NO)(OTf)(THF)]^+$ (see Experimental Section). The ^1H NMR spectrum of this mixture does not show well-resolved signals for the individual complexes. The ^{19}F NMR signal intensities are temperature dependent, and the results of a van't Hoff analysis for the two-step equilibrium process (eq 3) give $\Delta H_1 = -4.5(3)$ kcal/mol and $\Delta S_1 = -30(10)$ eu

$$\mathbf{1a} \overset{K_1}{\rightleftharpoons} [Cp^*Ru(NO)(OTf)(THF)]^+ + OTf^- \overset{K_2}{\rightleftharpoons} [Cp^*Ru(NO)(THF)_2]^{2+} + 2OTf^- \quad (3)$$

for K_1 and $\Delta H_2 = -4.1(1)$ kcal/mol and $\Delta S_2 = -20(10)$ eu for K_2 (Figure 4). At 293 K, the solution contains a ca. 3:6:1 mixture of **1a**, $[Cp^*Ru(NO)(OTf)(THF)]^+$, and $[Cp^*Ru(NO)(THF)_2]^{2+}$, respectively. The addition of 10 equiv of LiOTf to the THF solution of **1a** completely suppresses the ionization shown in eq 3. The IR spectra of **1a** or **1b** in THF show a single ν_{NO} absorption at 1850 cm^{-1} for both cases. Removal of solvent from these samples *in vacuo* and redissolution in CH_2Cl_2 cleanly regenerates **1a** or **1b** as shown by a single ^{19}F NMR resonance at δ −77.0.

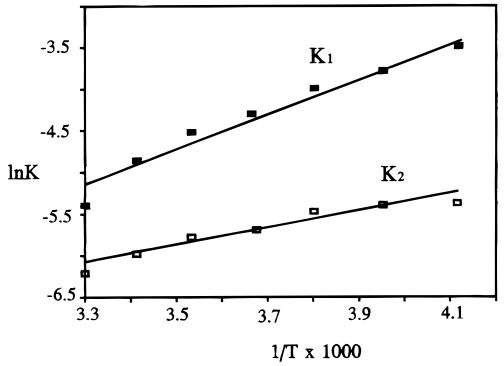

Figure 4. van't Hoff plots for the equilibrium of complex **1a** in THF.

Table 3. Selected Geometric Data for 2b[a]

Bond Lengths (Å)			
Ru−N	1.782(3)	S(2)−O(9)	1.428(3)
Ru−O(2)	2.128(3)	O(2)−H(2a)	0.90(8)
Ru−O(3)	2.141(3)	O(2)−H(2b)	0.71(7)
N−O(1)	1.150(5)	C−F_{ave}	1.32(1)
S(1)−C(6)	1.826(5)	$Cp^{\dagger}_{cent}$−Ru	1.85
S(1)−O(3)	1.477(3)	O(7)−H(2b)	1.92
S(1)−O(4)	1.426(3)	O(7)−O(2)	2.63
S(1)−O(5)	1.432(3)	O(2)−O(5a)	2.79
S(2)−C(7)	1.808(5)	O(8)−C(15)	3.25
S(2)−O(7)	1.449(3)	O(8)−H(15a)	2.41
S(2)−O(8)	1.429(3)	O(9)−C(15a)	3.13
Bond Angles (deg)			
N−Ru−O(2)	104.5(1)	O(5)−S(1)−C(6)	104.0(2)
N−Ru−O(3)	101.8(1)	Ru−O(3)−S(1)	128.2(2)
O(2)−Ru−O(3)	77.9(1)	H(2a)−O(2)−H(2b)	107(7)
Ru−N−O(1)	159.5(3)		
Least-Squares Planes			
[Ru,O(2),H(2a),H(2b)]	0.0954 Å[b]	angle to [Ru−N−O]	69.2°
Torsion Angles (deg)			
H(2a)−O(2)−Ru−N	101.4	H(2b)−O(2)−Ru−N	−26.4

[a] $Cp^{\dagger}_{cent}$ = centroid of η-$C_5(CH_3)_4(CH_2CH_3)$ ligand. [b] Deviation from planarity.

Isolation of Monoaqua Complex Salt 2b. Exposure of crystalline **1b** to atmospheric moisture results in a distinct color change from purple to red and the formation of a slightly tacky crystalline mass within 24 h. When ground in a Nujol mull, **2b** displays a strong ν_{NO} absorption at 1830 cm^{-1} in the IR spectrum. Dissolution of crystalline **2b** in CH_2Cl_2 results in the formation of purple solutions that display ^{19}F NMR signals comparable with the equilibrium shown in eq 1. X-ray diffraction results from a representative red crystal reveals a new triclinic unit cell characteristic of the monoaqua complex salt **2b** (Table 1). Selected geometric data for **2b** are presented in Table 3. Figure 5 shows the molecular structure to have one metal-bound OTf^- ligand and one OTf^- ion closely associated with the bound H_2O ligand. No disorder of the OTf^- species is apparent in the structure, with the average C−F distance being 1.31 Å and the average S−O

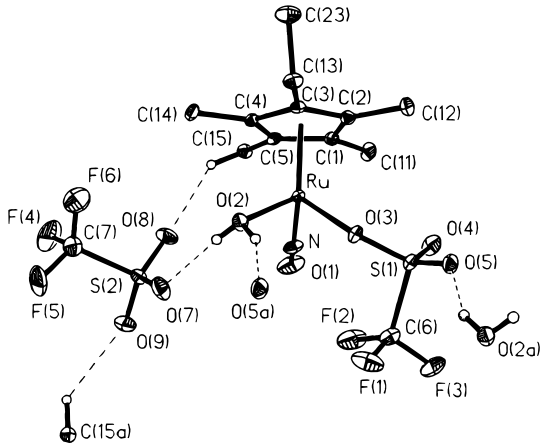

Figure 5. Thermal ellipsoid plot (30% probability level) and atom-numbering scheme for **2b**. Dashed lines indicate closest contacts in the lattice (see Table 3).

Table 4. Selected geometric data for 3b[a]

Bond Distances, Å			
Ru−N	1.783(9)	S(2)−O(5)	1.348(10)
Ru−O(2)	2.135(5)	S(2)−O(6)	1.429(8)
Ru−C(1)	2.186(9)	S(2)−C(30)	1.795(13)
Ru−C(2)	2.220(6)	C−F_{av}	1.25(3)
Ru−C(3)	2.221(6)	O(2)---O(6)	2.63
N−O(1)	1.125(12)	O(2)---O(3)	3.13
S(1)−O(4)	1.303(10)	O(2)---O(4)	3.26
S(1)−O(3)	1.359(13)	O(4)---C(13)	3.74
S(1)−C20)	1.76(2)	$Cp^{\dagger}_{cent}$−Ru	1.85
Bond Angles (deg)			
Ru−N−O(1)	160.6(9)	N−Ru−O(2)	103.1(8)
O(2)−Ru−O(2a)	82.9(7)	N−Ru−O(3)	100.9(9)

[a] $Cp^{\dagger}_{cent}$ = centroid of η-$C_5(CH_3)_4(CH_2CH_3)$ ligand.

distance being 1.44 Å. The O(8) and O(9) atoms bridge the C(15) methyl groups of the $Cp^{\dagger}$ rings on adjacent complexes, and the O(7) atom is associated with the bound H_2O ligand. The O(5) atom of the bound OTf^- ligand lies only 2.79 Å from the O atom of the H_2O ligand of a neighboring complex, forming an intermolecular H-bond. The location and isotropic refinement of the H(2a) and H(2b) atoms on O(2) was successful, showing the atoms of the [Ru−H_2O] moiety to deviate only 0.1 Å from planarity; this plane lies at a 69.2° angle with respect to a plane containing the [Ru−N−O] moiety that is bent to 160°.

Isolation of Diaqua Complex Salt 3b. Red, single-crystals of diaqua complex salt **3b** precipitate from H_2O-saturated (homogeneous) $CDCl_3$ solutions of **1b** at 25 °C. These crystals display a strong ν_{NO} absorption at 1815 cm^{-1} when ground in a Nujol mull. Redissolving crystalline **3b** in CH_2Cl_2 results in a purple solution containing an equilibrium mixture of **1b** (major), $\mathbf{2b}^+$, and $\mathbf{3b}^{2+}$ as monitored by ^{19}F NMR spectroscopy.

The X-ray parameters for **3b** are summarized in Tables 1 and 4, and the structure is presented in Figure 6. The complex cation adopts a piano-stool geometry with a crystallographically imposed mirror plane containing the [Ru−N−O] moiety. The Ru−O(2) bond length is 2.135(5) Å and the ∠Ru−N−O is 160.6(9)°. The H atoms were not clearly located in the electron density difference map. Nevertheless, the O(2)−O(4) distance of 2.62 Å shows one unique OTf^- ion (with S(2)) to strongly H-bond to the *cis*-diaqua ligands. The other unique OTf^- ion links the $[Cp^{\dagger}Ru(NO)]^{2+}$ cations in a 1-dimensional chain with the O(3)−O(2) separation being 3.15 Å. The O(4) position of this OTf^- ion is

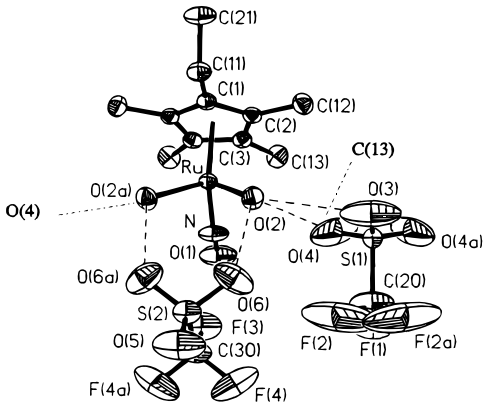

Figure 6. Thermal ellipsoid plot for **3b** (30% probability level) and atom-numbering scheme. Dashed lines indicate closest contacts in the lattice (see Table 4).

Table 5. Selected Geometric Data for 4b[a]

Bond Distances, Å			
Ru−N	1.788(4)	C(6)−F(3)	1.325(7)
Ru−O(2)	2.069(3)	Cp_{cent}−Ru	1.85
O(1)−N	1.147(5)	Ru−Ru(a)	3.185
O(2)−H(2)	0.76(2)	O(2)---O(2a)	2.39
S−O(3)	1.436(4)	O(2)---O(3)	2.01
S−O(4)	1.416(4)	O(2)---O(5)	2.76
S−O(5)	1.454(4)	F(2)---C(11)	3.44
S−C(6)	1.810(6)	F(2)---H(11a)	2.53
C(6)−F(1)	1.340(7)	O(5)---H(2)	2.01
C(6)−F(2)	1.287(7)		
Bond Angles (deg)			
Ru−N−O(1)	160.0(3)	Ru−O(2)−RuA	100.6(1)
N−Ru−O(2)	102.8(1)	N−Ru−O(2A)	104.8(1)
O(2)−Ru−O(2A)	70.5(1)		

[a] $Cp^{\dagger}_{cent}$ = centroid of η-$C_5(CH_3)_4(CH_2CH_3)$ ligand.

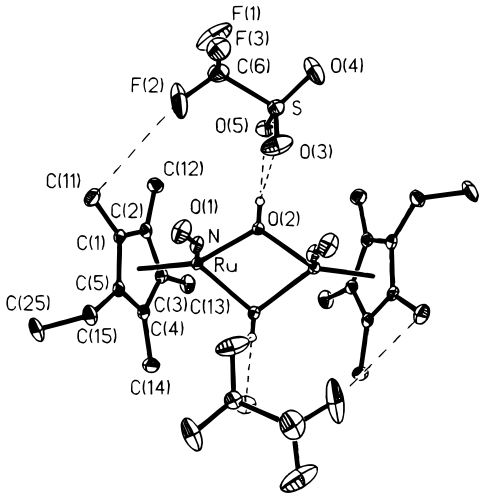

Figure 7. Thermal ellipsoid plot (30% probability level) and atom-numbering scheme for **4b**. Dashed lines indicate closest contacts in the lattice (see Table 5).

located 3.74 Å from the C(13) methyl group of a $[Cp^{\dagger}Ru(NO)]^{2+}$ cation in an adjacent chain.

Isolation of μ-Hydroxy Complex Salts 4a,b. The complex salts $[Cp'Ru(NO)(\mu\text{-}OH)]_2[OTf]_2$ (**4a,b**) can be preferentially extracted from aqueous solutions of **1a,b** by CH_2Cl_2. Alternatively, **4a,b** precipitate directly from concentrated aqueous solutions of **1a** or **1b**. A single-crystal X-ray analysis of **4b** is summarized in Tables 1 and 5**.** Figure 7 shows the molecule to be a C_2-symmetric *cis*-dinuclear complex situated about a 2-fold crystal axis. The nonbonded Ru−Ru separation is 3.185 Å with the $[Ru_2(\mu\text{-}OH)_2]$ dihedral butterfly angle about

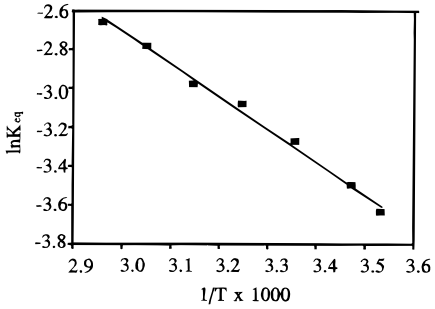

Figure 8. van't Hoff plot for the equilibration of the isomers of **4b**$^{2+}$ in 1,2-dichloroethane.

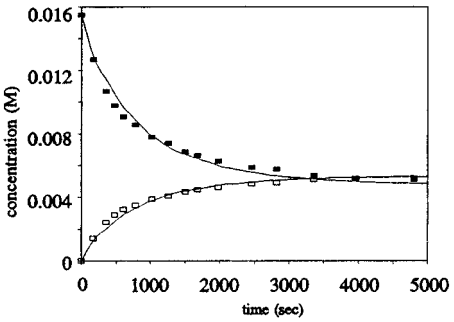

Figure 9. Kinetics of the equilibration of **3a**$^{2+}$ and **4a**$^{2+}$ in H_2O (solid line = simulation; ■ = [**3a**]; □ = [**4a**]).

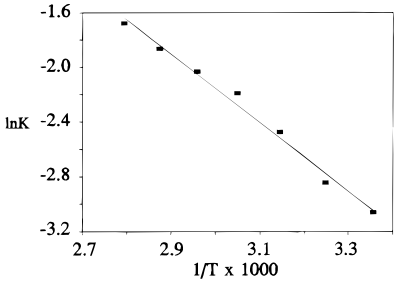

Figure 10. van't Hoff plot for the equilibrium 2 **3a**$^{2+}$ ⇄ **4a**$^{2+}$ + $2H_3O^+$.

the Ru−Ru vector being 129°. The NO ligands are located opposite to the butterfly angle. The plane containing the [H(2a)−O(2)−Ru] moiety forms an angle of 73° with the plane containing the [Ru−N−O(1)] linkage bent to 160°. The OTf^- ions are not disordered and are closely associated to the dinuclear cation to form an intramolecular bridge between the μ-OH^- ligand and a C(11) methyl group of the $Cp^\dagger$ ligand. The H atoms were located and isotropically refined, showing the O(2)−H(2) distance to be 0.76 Å and the O(3) and O(5) atoms of the OTf^- ion to straddle H(2a) at 2.01 and 2.76 Å, respectively. The F(2) atom is 2.53 Å from the H(11a) atom on C(11) with the C(11)-F(2) distance being 3.33 Å. There are no significant intermolecular contacts between the $[Cp^\dagger Ru(NO)(\mu\text{-}OH)]_2[OTf]_2$ units.

Dichloromethane solutions of **4a,b** display strong ν_{NO} IR absorptions at 1795 and 1799 cm^{-1}, respectively. The ^1H NMR spectra of these solutions show the presence of a major Cp′ environment (95%) and a minor Cp′ environment (5%). The relative intensity of the major and minor Cp′ signals for **4b** are temperature dependent, and a van't Hoff treatment of the ^1H NMR data for **4b** in 1,2-dichloroethane is linear over a 60 °C range to give $\Delta H = 0.8(2)$ kcal/mol and $\Delta S = 1(5)$ eu (Figure 8). The relative area of the minor resonance increases to 10% when **4b** is dissolved in a 50/50 mixture of toluene/CH_2Cl_2. The hydroxyl ligands of **4a,b** appear as singlets at δ 4.42 and 4.47, respectively, and the addition of 1 μL of D_2O to CH_2Cl_2 solutions of **4a,b** causes the hydroxyl proton signals to disappear immediately upon mixing. The addition of excess HOTf to **4a,b** in CH_2Cl_2 leads to the quantitative re-formation of **1a,b** as monitored by ^1H NMR spectroscopy.

Reactivity of 1a with Water. Complex **1a** readily dissolves in water to form an acidic red-orange solution (λ_{max} = 377 nm) that displays a single ^{19}F NMR resonance at δ −78.0 that is coincident with free OTf^-. The molar conductance of a formally 7.0×10^{-3} M aqueous solution of **1a** is 286 Ω^{-1} cm^{-1} mol^{-1} and does not change upon dilution. The potentiometric titration of **1a** in H_2O with standardized aqueous NaOH leads to a curve typical for a weak acid/strong base process and shows a $pK_a = 2.7$ for **1a**. A freshly prepared sample of **1a** in H_2O displays Cp* signals at δ 1.84 (labeled as species **3a**$^{2+}$) and δ 1.76 (labeled as species **4a**$^{2+}$) in the ^1H NMR spectrum. Over time the initial intensity of **3a**$^{2+}$ decreases with a corresponding increase in the intensity of **4a**$^{2+}$ until equilibrium is reached in ca. 2 h at 25 °C (λ_{max} shifted slightly to 382 nm).

A representative kinetic profile for the equilibration of species **3a**$^{2+}$ and **4a**$^{2+}$ (eq 4) as monitored by ^1H NMR spectroscopy in H_2O solvent is presented in Figure 9.

$$2\ \mathbf{3a}^{2+} \underset{k_r}{\overset{k_f}{\rightleftharpoons}} \mathbf{4a}^{2+} + 2H_3O^+ \qquad (4)$$

In this case the starting solution is formally 1.5×10^{-2} M solution of **1a** in H_2O, and trials with initial **1a** concentrations of 1.0×10^{-2} M and 2.0×10^{-2} M give similar profiles. The results of a KINSIM analysis are also plotted.[19] The parameters for this simulation are the initial concentration of **3a**$^{2+}$, the stoichiometry in eq 4, and initial estimates for k_f and k_r. The best fit of the experimental data gives $k_f = 0.04$ M^{-1} s^{-1} and k_r = 1.0 M^{-2} s^{-1} after an iterative process. The rate constants at the higher and lower initial concentrations of **1a** are the same within 20%.

After equilibration at 298 K, a formally 0.005 M solution of **1a** in water contains a ca. 5:2 ratio of **4a**$^{2+}$ to **3a**$^{2+}$. Monitoring the ^1H NMR spectra of thermally-equilibrated solutions of **1a** in H_2O (eq 4) between 298 and 358 K leads to good van't Hoff behavior, yielding the equilibrium thermodynamic values of $\Delta H = 5.0(3)$ kcal/mol and $\Delta S = 11(5)$ eu for eq 4 (Figure 10).

Addition of 0.5 equiv of NaCl to a 4.0×10^{-3} M solution of **1a** in H_2O produces signals at δ 1.84 (**3a**$^{2+}$), δ 1.81 ($[Cp^*Ru(NO)(OH_2)(Cl)]^+$), δ 1.80 ($Cp^*Ru(NO)Cl_2$), and δ 1.76 (**4a**$^{2+}$) in a ca. 3:25:2:70 ratio in the ^1H NMR spectrum. The ^1H NMR Cp* resonance of the **4a**$^{2+}$ ion is not affected by the change of OTf^- to Cl^-. Addition of 1.5 equiv of NaCl causes the δ 1.84 signal (**3a**$^{2+}$) to disappear completely, and after the addition of 2.5 equiv of NaCl, the remaining resonances at δ 1.81 ($[Cp^*Ru(NO)(OH_2)Cl]^+$), 1.80 ($Cp^*Ru(NO)Cl_2$), and 1.76 (**4a**$^{2+}$) appear in a ca. 25:45:30 ratio. The solution at this point shows a λ_{max} of 560 nm.

Reactivity of $[Cp'Ru(NO)(\mu\text{-}OH)]_2[OTf]_2$ (4a,b). When equimolar amounts of **4a** and **4b** are dissolved together in H_2O, the residue after solvent removal contains a 1:1:2 mixture of **4a**, **4b**, and a new crossover

(19) Barshop, B. A.; Wrenn, R. F.; Frieden, C. *Anal. Biochem.* **1983**, *130*, 134−145. The program is available via internet: anonymous login to WUARCHIVE.WUSTL.EDU; subdirectory, Package/KINSIM/DOS.

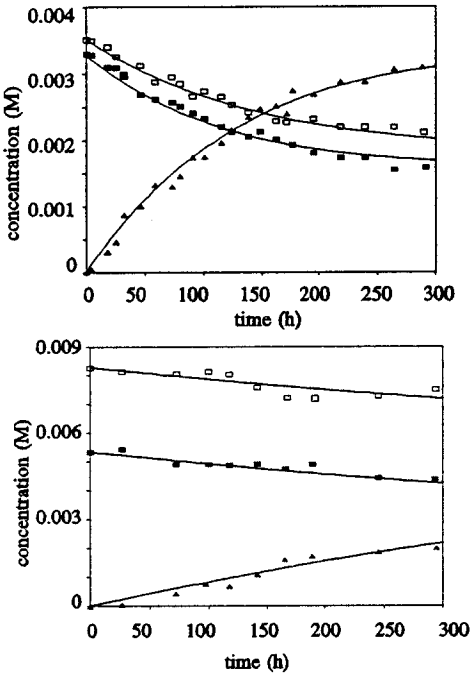

Figure 11. Kinetics of equilibration of $\mathbf{4a}^{2+} + \mathbf{4b}^{2+} \rightleftarrows \mathbf{4c}^{2+}$ in CH_2Cl_2 (solid line = simulation; ■ = [**4a**]; □ = [**4b**]; ▲ = [**4c**].

species $[(Cp^*Ru(NO))(Cp^\dagger Ru(NO))(\mu\text{-}OH)_2][OTf]_2$ (**4c**) identifiable by a new ^1H NMR hydroxyl signal at δ 4.45 in CH_2Cl_2. No new Cp* or $Cp^\dagger$ ^1H NMR signals are resolvable from those seen for $\mathbf{4a}^{2+}$ or $\mathbf{4b}^{2+}$. The product **4c** is also obtained when equimolar amounts of **1a** and **1b** are mixed in H_2O. The rate of the formation of **4c** when equimolar amounts of **4a** and **4b** are allowed to stand in CH_2Cl_2 is dependent upon the amount of H_2O in the solvent. The observed kinetic data for the formation of **4c** from a mixture of **4a** and **4b** in 0.1 M H_2O/CH_2Cl_2 is shown in Figure 11a. The KINSIM simulation of the equilibration, starting from the initial concentrations of **4a** and **4b** and eq 5, is compared to

$$\mathbf{4a}^{2+} + \mathbf{4b}^{2+} \underset{k_r}{\overset{k_f}{\rightleftharpoons}} 2\ \mathbf{4c}^{2+} \qquad K_{eq} = 4 \tag{5}$$

the experimental data.[19] The iterative estimation of k_f and k_r shows a best fit with $k_f = 3.2 \times 10^{-4}\ M^{-1}\ s^{-1}$ and $k_r = 8.0 \times 10^{-5}\ M^{-1}\ s^{-1}$. The rate of equilibration is ca. 1 order of magnitude slower in rigorously dried CH_2Cl_2, with $k_f = 2.2 \times 10^{-5}\ M^{-1}\ s^{-1}$ and $k_r = 5.5 \times 10^{-6}\ M^{-1}\ s^{-1}$ (Figure 11b).

Aqueous solutions of **4a** are weakly acidic, leading to a determined pK_a of 5.5 by titration with standardized aqueous NaOH. Aqueous solutions of **4a** show only one Cp* environment by ^1H and ^{13}C NMR spectroscopy, with the major/minor isomer pair not being resolvable in H_2O. The putative conjugate base $[(Cp^*)_2Ru_2(NO)_2(\mu\text{-}OH)(\mu\text{-}O)]^+$ resulting from the deprotonation of $\mathbf{4a}^{2+}$ is not detected by NMR spectroscopy even at pH = 11.

Addition of NaOD to D_2O solutions of **4a,b** results in the gradual decrease of the intensity of the methyl signals of the Cp* and $Cp^\dagger$ ligands with the corresponding development of broad, low-intensity high-field shoulders adjacent to the CH_3 singlets over time. The signals from the ethyl group of the $Cp^\dagger$ ligand in $\mathbf{4b}^{2+}$ remain unaffected. $t_{1/2}$ of the methyl signal decreases from 3.5 d at pD = 6 to 4 h at pD = 7 to 0.4 h at pD = 11. Subsequent neutralization of the pD = 11 solutions with DCl after 24 h gives a green residue identified as the isotopically labeled d_{15}-Cp*Ru(NO)$(Cl)_2$ and d_{12}-$Cp^\dagger$Ru-$(NO)(Cl)_2$ complexes by ^2H NMR spectroscopy (eqs 6 and 7). Treatment of the ^2H-labeled complexes with a large

$$\mathbf{4a} \xrightarrow{D_2O} d_{30}\text{-}\mathbf{4a} \xrightarrow{D_2O/NaCl} d_{15}\text{-Cp*Ru(NO)Cl}_2 \tag{6}$$

$$\mathbf{4b} \xrightarrow{D_2O} d_{24}\text{-}\mathbf{4b} \xrightarrow{D_2O/NaCl} d_{12}\text{-Cp}^\dagger\text{Ru(NO)Cl}_2 \tag{7}$$

excess of H_2O at pH = 8 results in the quantitative regeneration of the ^1H-labeled complexes. The signals of $\mathbf{4a}^{2+}$ or $\mathbf{4b}^{2+}$ in H_2O at pH = 9 do not change measurably over a period of 3 d. Adjustment of the pH above 12 causes the gradual precipitation of a brown, intractable material that does not show any detectable ν_{NO} signal in the IR spectrum.

Treatment of a 3.0×10^{-3} M aqueous solution of **4a** with 2 equiv of HCl causes a rapid color change from yellow to green (λ_{max} = 560 nm), and the ^1H NMR spectrum reveals 3 resonances in a 10:50:40 ratio representing $[Cp^*Ru(NO)(OH_2)Cl]^+$ (δ 1.81), Cp*Ru-$(NO)Cl_2$ (δ 1.80), and $\mathbf{4a}^{2+}$ (δ 1.76), respectively. The treatment of a 3×10^{-3} M solution of **4a** with 2 equiv of NaCl results in no detectable reaction after 1 h, but the addition of 100 equiv of NaCl causes a color change to green within 5 min and the appearance of the single ^1H NMR resonance at δ 1.80 attributed to Cp*Ru(NO)-Cl_2.

Aqueous Chemistry of Cp′Ru(NO)Cl$_2$. At 25 °C, Cp*Ru(NO)Cl_2 dissolves in water to a formal concentration of 5.9×10^{-3} M. This saturated solution has a pH of 3.4, and the λ_{max} of 560 nm is only slightly lower than the value of 580 nm observed for Cp*Ru(NO)Cl_2 dissolved in CH_2Cl_2. The molar conductance of this solution is 50 $\Omega^{-1}\ cm^{-1}\ mol^{-1}$ and increases significantly to 117 $\Omega^{-1}\ cm^{-1}\ mol^{-1}$ upon dilution to 1.8×10^{-4} M. The ^1H NMR spectrum of this solution shows three signals. On the basis of the aqueous reactivity of **3a** and **4a** with Cl^- (vide supra), we can assign these signals to $[Cp^*Ru(OH_2)Cl]^+$ (δ 1.81), Cp*Ru(NO)Cl_2 (δ 1.80), and $\mathbf{4a}^{2+}$ (δ 1.76), in a 10:10:1 ratio, respectively. Dilution to 3.6×10^{-4} M results in a corresponding 5:3:2 integral ratio for these signals, and the λ_{max} of this solution is at 545 nm.

The addition of HCl to a formally 5.9×10^{-3} M solution of Cp*Ru(NO)Cl_2 in H_2O causes the resonance due to Cp*Ru(NO)Cl_2 (δ 1.80) to increase while the resonances due to $[Cp^*Ru(NO)(OH_2)Cl]^+$ (δ 1.81) and $\mathbf{4a}^{2+}$ (δ 1.76) decrease together in a fixed 10:1 ratio. After the addition of 10 equiv of HCl, only the signal of Cp*Ru(NO)Cl_2 remains. When 8 equiv of NaCl is added to a 5.9×10^{-3} M aqueous solution of Cp*Ru-$(NO)Cl_2$, only the ^1H NMR signal of Cp*Ru(NO)Cl_2 is detected. During the addition of HCl or NaCl, isosbestic points at 480 and 544 nm appear and the λ_{max} shifts to 573 nm. Over a period of 2−3 days at 25 °C, solutions containing 10 or more equiv of HCl or NaCl eventually deposit green crystals of Cp′Ru(NO)Cl_2.

Addition of 1 equiv of NaOH to a formally 5.9×10^{-3} M aqueous solution of Cp*Ru(NO)Cl_2 results in a color change to yellow (λ_{max} = 370 nm) and the appearance of ^1H NMR resonance of $\mathbf{4a}^{2+}$ (δ 1.76). The addition of 1 equiv of HCl restores the green color of the solution and results in the appearance of ^1H NMR signals from $[Cp^*Ru(NO)(OH_2)Cl]^+$ (δ 1.81), Cp*Ru(NO)Cl_2 (δ 1.80), and $\mathbf{4a}^{2+}$ (δ 1.76) in a 15:80:5 ratio, respectively. Addition of 10 equiv of HOTf to a formally 5.9×10^{-3}

M aqueous solution of $Cp^*Ru(NO)Cl_2$ results in the disappearance of **4a**$^{2+}$ in the ^1H NMR spectrum, leaving $[Cp^*Ru(NO)(OH_2)Cl]^+$ and $Cp^*Ru(NO)Cl_2$ in a ca. 2:1 ratio.

When $Cp'Ru(NO)Cl_2$ is dissolved in D_2O and monitored by ^1H NMR spectroscopy, the signals of the Cp′ methyl groups gradually lose intensity with the simultaneous development of broad, high-field shoulders. This is most easily monitored in the case of $Cp^\dagger Ru(NO)Cl_2$, where the signals of the methyl singlets eventually disappear completely but the signals of the Cp†-ethyl group remain unaffected. A corresponding growth in the ^2H signals for the methyl groups is observed in the ^2H NMR spectrum. The $t_{1/2}$ for the disappearance of the methyl signals is 42 h at 25 °C (eq 8). When 1.5

$$Cp^*Ru(NO)Cl_2 \xrightarrow{D_2O} d_{15}\text{-}Cp^*Ru(NO)Cl_2 \qquad (8)$$

$$Cp^*Ru(NO)Cl_2 \xrightarrow{DCl/D_2O} \text{no reaction} \qquad (9)$$

equiv of NaOD is added to a fresh solution of Cp′Ru(NO)Cl_2 in D_2O, the $t_{1/2}$ for the loss of the methyl group signals decreases to 8 h. When a fresh D_2O solution of Cp′Ru(NO)Cl_2 is treated with 10 equiv of DCl, no changes in the ^1H NMR spectrum are observed over a period of 7 d (eq 9). The addition of 10 equiv of NaCl to $Cp^*Ru(NO)Cl_2$ in D_2O raises the pD by 0.6 units, but the rate of the loss of the methyl group signals in the ^1H NMR spectrum does not change significantly.

Discussion

Ligand Coordination to the $[Cp'Ru(NO)]^{2+}$ Fragment. A careful evaluation of the competition between species like OTf^-, Cl^-, H_2O, and OH^- ligands in organometallic complexes is especially important if the generation of a coordinatively unsaturated metal center is to be well-understood. The combination of spectral and X-ray structural data available makes it possible to closely assess the nature of ligand interactions with the $[Cp'Ru(NO)]^{2+}$ fragment. The NO ligand provides important information through its characteristic ν_{NO} values in nonaqueous conditions and the angle it forms when binding to the Ru center.

While most previous studies have established the metal−OTf interaction to be primarily ionic in nature,[2b,14a] the OTf^- ligands in **1b** and **2b** exhibit significant bond length changes upon binding to the electrophilic $[Cp'Ru(NO)]^{2+}$ center. The structure of **1b** clearly shows the S(1)−O(2) and S(2)−O(5) bonds to be ca. 0.03 Å elongated from that seen in "free" OTf^- ions;[20] the S(1)−O(3) and S(2)−O(7) bond lengths of ca. 1.35 Å represent essentially localized S=O double bonds. The S(1)−O(4) and S(2)−O(6) bond lengths of 1.430(9) and 1.46(1) Å are consistent with the weak H-bonding interactions with these oxygen atoms in the crystal lattice. The X-ray structure of **2b** is particularly illustrative because both bound and "free" OTf^- ligands are present. Therein, the S(1)−O(3) bond distance of 1.477(3) Å is significantly elongated compared to an average 1.43 Å S−O distance in the outer-sphere OTf^- ion. The relatively short (1.426 Å) S(1)−O(4) bond distance in the bound OTf^- shows somewhat less localization of S=O double-bond character than seen in **1b**. This may be due to the positive charge on the complex.[21] The short Ru−O bond lengths in complexes **1b** and **2b** are comparable to the 2.15 Å distance found in Cp*Ru(NO)(Ph)(OTf) and are among the shortest reported Ru(II)−oxygen distances.[11]

The inspection of the ν_{NO} values for **1a,b** suggests that a OTf^- ligand possesses somewhat different donor properties from a chloride ligand. The ν_{NO} values for **1a,b** are ca. 56 cm^{-1} higher that in the corresponding Cp′Ru(NO)Cl_2 complexes.[12a] Following the work of Beck and others,[2g] the relatively high ν_{NO} values observed for **1a,b** might suggest weakly- or nonbonded OTf^- ligands and a $[Cp'Ru(NO)(solvent)]^{2+}$ description with outer-sphere OTf^- ions. Without supporting evidence, this could be considered reasonable only if the π-donor ability of the Cl^- ligand is ignored.[18] The ability of Cl^- to π-donate can be expected to lower the ν_{NO} energy, whereas the strong π-withdrawing power anticipated for the $-SO_2CF_3$ moiety in the OTf^- case would be expected to diminish the π-donor ability of the OTf^- donor O atom and cause the ν_{NO} energy to be relatively higher. Similar shifts are observed in the IR spectra for $Cp^*Fe(CO)_2Cl$ and $Cp^*Fe(CO)_2(OTf)$.[2b]

The ∠Ru−N−O of ca. 160° in the structures of **2b** and **3b** and the corresponding decrease in the ν_{NO} energies from **1b** to **2b** to **3b** can be attributed to the presence of the H_2O ligands. The 21 cm^{-1} reduction in ν_{NO} from **1b** to **2b** and 15 cm^{-1} reduction from **2b** to **3b** suggests increasing π-donation with increasing number of aqua ligands. The H_2O ligand is poised for both σ- and π-donation to the Ru center. The structure of **2b** clearly shows a tightly bound H_2O ligand in a "planar" conformation, with the $[Ru-OH_2]$ moiety deviating from planarity by only 0.1 Å. The NO ligand responds significantly, backing away from formal 3-electron (linear Ru−NO) donation toward a 1-electron (bent Ru−NO) configuration. The torsion angles about the Ru−O(2) bond further support that the NO ligand is backing away from the p-π-orbital perpendicular to the OH_2 plane. In the structure of **3b** the NO ligand is bent back in a symmetric disposition from the two H_2O ligands, lying in the mirror plane that bisects the $[Cp^\dagger Ru(NO)]$ fragment.

The ca. 2.6 Å distance between the O atoms of the aqua ligands and the nearest noncoordinated triflate oxygen atoms in **2b** and **3b** clearly indicates the existence of moderately strong H-bonds in the solid state in comparison to other characterized H-bonding interactions.[22] Much weaker interactions are observed between the OTf^- ions and the CH_3 groups of the Cp′ ligands, leading to an extended packing array in the crystal lattice.

Structural Aspects of the μ-Hydroxyl Complex 4b. The ∠Ru−N−O in **4b** is 160°, indicating significant π-donation from the μ-hydroxyl ligands. The close association of the OTf^- counterions leads to the formation of discrete $[Cp^\dagger Ru(NO)(\mu\text{-}OH)]_2[OTf]_2$ units in the solid state. Two O atoms of the SO_3 group effectively chelate the H atom of the μ-OH ligand, and a significant interaction occurs between an F atom of the CF_3 group and an H atom of a CH_3 group on the Cp† ligand.

Substitution of Coordinated OTf^- in Nonaqueous Solvents. An important issue in the study of reactive electrophilic metal centers is the generation of

(20) Peng, S.-M.; Ibers, J. A.; Millar, M.; Holm, R. H. *J. Am. Chem. Soc.* **1976**, *98*, 8037.

(21) A similar pattern of bond lengths is also reported (but not interpreted) in refs 2d−e.

coordination unsaturation. With OTf^- ions being widely regarded as particularly weak ligands, our major concern has been to analytically characterize the competition between OTf^- binding and that of donor species like H_2O and THF. Without the use of spectral probes like those presented in this study, it is extremely difficult to discriminate between the species present in solution and those that crystallize from solution.

The equilibrium shown in eq 1 demonstrates that even though H_2O in CH_2Cl_2 does displace the OTf^- ligand in a sequential process, the major species in solution is undissociated **1a**. This type of behavior is similar to that reported for $Re(CO)_5(OTf)$[14] but is contradictory to the reported behavior of *trans*-$Rh(PPh_3)_2(CO)(OTf)$.[15,23] Interestingly, the equilibrium in eq 2 shows that even though Cl^- is a stronger ligand than OTf^-, OTf^-/Cl^- exchange readily occurs. In neat THF, the equilibrium in eq 3 shows a relatively larger concentration of the $[Cp'Ru(NO)(OTf)(THF)]^+$ and $[Cp'Ru(NO)(THF)_2]^{2+}$ ions. It is clear from the van't Hoff analyses of eqs 1−3 that substitution of OTf^- is consistently exothermic. Nevertheless, the negative ΔS values show there is a large entropic cost when OTf^- is released from the coordination sphere. In eqs 1 and 3, this is consistent with the entropy decrease associated with the formation of a more-ordered solvent cage in connection with the newly formed ion pair. The negative ΔS values for the equilibria shown in eq 2 would correlate with the solvation of the larger OTf^- ion as compared to the Cl^- ion.

The apparent coincidence of the ν_{NO} energies of the $Cp'Ru(NO)(OTf)_2$, $[Cp'Ru(NO)(OTf)(THF)]^+$, and $[Cp'Ru(NO)(THF)_2]^{2+}$ species when **1a,b** is dissolved in THF is similar to the situation when the $Cp^*Ru(NO)(R)(OTf)$ complexes are dissolved in THF ($R = CH_3$, C_6H_5).[9] As before, we ascribe this to the counterbalancing of two effects: the tendency for the ν_{NO} values to shift to higher energy in the cationic cases and the apparent ability of THF to be a significant π-donor (like H_2O) to the [Ru−NO] moiety.[24]

Aqueous Chemistry of the $[Cp'Ru(NO)]^{2+}$ Fragment. Complexes **1a,b** are strong electrolytes in H_2O, leading to the initial formation of $\mathbf{3a}^{2+}$ or $\mathbf{3b}^{2+}$ followed by the equilibration to $\mathbf{4a}^{2+}$ or $\mathbf{4b}^{2+}$ (eq 4). The rather electrophilic nature of the $[Cp'Ru(NO)]^{2+}$ moiety leads to a pK_a of 2.7 for $\mathbf{3a}^{2+}$. Similar to metals with low pK_a values (e.g., Al^{3+}, V^{3+}, and Ga^{3+}), the formation of polynuclear complexes with μ-OH ligands is not unexpected.[25] Somewhat higher pK_a values are reported for a large variety half-sandwich organometallic aqua complexes.[9k] The temperature dependence of the equilibrium between $\mathbf{3a}^{2+}$ and $\mathbf{4a}^{2+}$ (eq 4, Figure 8) shows that monomer → dimer conversion is endothermic and that the bonding in the $[Ru_2(\mu\text{-}O)_2]$ core does not compensate for the liberation of the two H^+ ions required per dimer formed. The positive ΔS value reflects the fact that the number of solvated OTf^- ions does not change and the number of solute species increases by 50%. The conversion of $\mathbf{3a}^{2+}$ to $\mathbf{4a}^{2+}$ is slow enough to permit a kinetic analysis shown in Figure 7. A simulation of the observed rate of equilibration agrees well with eq 4 being second-order in $\mathbf{3a}^{2+}$ and first-order in $\mathbf{4a}^{2+}$.

Potentiometric titration results in H_2O show the pK_a of **4a** to be 5.5. This is considerably higher than the pK_a of $\mathbf{3a}^{2+}$ and indicative of the μ-OH proton being less acidic than bound H_2O. Attempts to generate spectroscopically detectable amounts of $[Cp'_2Ru_2(NO)_2(\mu\text{-}O)(\mu\text{-}OH)]^+$ have so far been unsuccessful (vide infra).

The conversion of monomeric $\mathbf{3a}^{2+}$ to dimeric $\mathbf{4a}^{2+}$ suggests the intermediacy of an undetected $[Cp^*Ru(NO)(OH_2)(OH)]^+$ complex. The observation of crossover between $\mathbf{4a}^{2+}$ and $\mathbf{4b}^{2+}$ in H_2O to give the mixed $Cp^*/Cp^\dagger$ dimer $\mathbf{4c}^{2+}$ also requires a similar aqua−hydroxy monomeric species. The fact that $\mathbf{4a}^{2+}/\mathbf{4b}^{2+}$ crossover is inhibited under basic conditions shows that the opening of the μ-OH linkage in $\mathbf{4a}^{2+}$ and $\mathbf{4b}^{2+}$ requires the addition of H_3O^+. In comparison to the reaction in 0.1 M H_2O in CH_2Cl_2, the crossover of **4a** and **4b** is extremely slow in "dry" CH_2Cl_2; the observation of any crossover in this case most likely reflects our inability to remove all adventitious H_2O from the reaction vessel. The extremely sluggish nature of these reactions has hampered our attempts to determine the exact order of H_2O.

It is apparent that the *cis*/*trans*-interconversion of the dimers $\mathbf{4b}^{2+}$ is not affected by pH or the presence of H_2O. We base our assignment of *cis*-$\mathbf{4b}^{2+}$ being the major isomer in CH_2Cl_2 and 1,2-dichloroethane by the increase in the minor ^1H NMR resonance when the solvent polarity is decreased by the addition of toluene. The *trans*-structure would likely be less polar than the *cis*-isomer.[26]

The immediate treatment of freshly prepared solutions of **1a** with less than 1 equiv of NaCl results in the observation of four species identified as $\mathbf{3a}^{2+}$, $\mathbf{4a}^{2+}$, $[Cp^*Ru(NO)(OH_2)(Cl)]^+$, and $Cp^*Ru(NO)Cl_2$ (eq 10).

$$\mathbf{1a} \xrightarrow{\text{NaCl(aq)}} \mathbf{3a}^{2+} + \mathbf{4a}^{2+} + [Cp^*Ru(NO)(OH_2)(Cl)]^+ + Cp^*Ru(NO)Cl_2 \quad (10)$$

$$\mathbf{4a} + \text{excess HCl} \rightarrow 2Cp^*Ru(NO)Cl_2 \quad \text{(fast)} \quad (11)$$

$$\mathbf{4a} + \text{excess NaCl} \rightarrow 2Cp^*Ru(NO)Cl_2 \quad \text{(slow)} \quad (12)$$

Cleavage of the dimer $\mathbf{4a}^{2+}$ to give $Cp^*Ru(NO)Cl_2$ occurs

(22) (a) Seligson, A. L.; Cowan, R. L.; Trogler, W. C. *Inorg. Chem.* **1991**, *30*, 3371. (b) Koelle, U.; Flunkert, G.; Gorissen, R.; Schmidt, M. U.; Englert, U. *Angew. Chem., Int. Ed. Engl.* **1992**, *31*, 440. (c) Kegley, S. E.; Schaverien, C. J.; Freudenberger, J. H.; Bergman, R. G. *J. Am. Chem. Soc.* **1987**, *109*, 6563. (d) Fawzi, R.; Hiller, W.; Lorenz, I.-P.; Mohyla, J.; Zeiher, C. *J. Organomet. Chem.* **1984**, *262*, C43. (e) Bertrand, J. A.; Black, T. D.; Eller, P. G.; Helm, F. T.; Mahmood, R. *Inorg. Chem.* **1976**, *12*, 2965. (f) van Driel, G. J.; Driessen, W. L.; Reedijk, J. *Inorg. Chem.* **1985**, *24*, 2919. (g) Emsley, J. *J. Chem. Soc. Rev.* **1980**, 91. (h) Olovsson, I.; Jonsson, P. In *The Hydrogen Bond*; Schuster, P., Zundel, G., Sandorfy, C., Eds.; North-Holland: New York, 1976; Chapter 8. Review of hydrogen bonding and its classification: (i) Gilli, P.; Bertolasi, V.; Ferretti, V.; Gilli, G. *J. Am. Chem. Soc.* **1994**, *116*, 909. (j) Steed, J. W.; Tocher, D. A. *J. Chem. Soc., Chem. Commun.* **1991**, 1609. (k) Winter, C. H.; Sheridan, P. H.; Heeg, M. J. *Inorg. Chem.* **1991**, *30*, 1962. (l) Alster, P. L.; Baeskjou, P. J.; Jannsen, M. D.; Kooijman, H.; Sicher-Roetman, A.; Spek, A. L.; van Koten, G. *Organometallics* **1992**, *11*, 4124. (m) Fryzuk, M. D.; MacNeil, P. A.; Rettig, S. J. *J. Am. Chem. Soc.* **1987**, *109*, 2803. (n) Osterberg, C. E.; King, M. A.; Arif, A. M.; Richmond, T. G. *Angew. Chem., Int. Ed. Engl.* **1990**, *29*, 888. (o) Antolini, L.; Benedetti, A.; Fabretti, A. C.; Giusti, A. *Inorg. Chem.* **1988**, *27*, 2192. (p) Osterberg, C. E.; Arif, A. M.; Richmond, T. G. *J. Am. Chem. Soc.* **1988**, *110*, 6903.

(23) A reinvestigation of the solvolytic behavior of *trans*-$Rh(PPh_3)_2(CO)(OTf)\cdot H_2O$ shows evidence that H_2O does not displace the OTf^- ligand in CH_2Cl_2 solution: Svetlanova-Larsen, A.; Hubbard, J. L. *Inorg. Chem.* **1996**, *35*, 3073.

(24) The structure of the $[Cp^*Ru(NO)(CH_3)(THF)]^+$ cation (as the $B(3,5\text{-}(CF_3)_2C_6H_3)_4^-$ salt) shows a coordination geometry very similar to the $[Cp^\dagger Ru(NO)(OTf)(OH_2)]^+$ cation and an ∠Ru−N−O of 159°: Hubbard, J. L.; Yi, G.-B. Manuscript in preparation.

(25) Burgess, J. *Metal Ions in Solution*; John Wiley & Sons: New York, London, Sydney, Toronto, 1978.

(26) Solvent dependence of the *cis*−*trans* isomer populations is well-known. See Farrugia, L. J.; Mustoo, L. *Organometallics* **1992**, *11*, 2941 and references therein.

Scheme 1

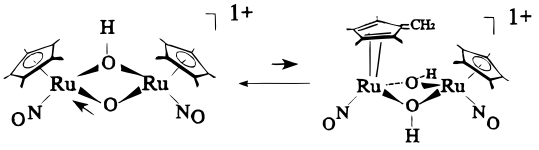

readily when **4a** is dissolved in aqueous HCl (eq 11) but much more slowly when **4a** is dissolved in aqueous NaCl (eq 12). As in the case of the crossover observed between $\mathbf{4a}^{2+}$ and $\mathbf{4b}^{2+}$ to give $\mathbf{4c}^{2+}$, opening of the dinuclear $[Ru_2(\mu\text{-}OH)_2]^{2+}$ core requires the addition of H_3O^+.

It is possible to approach an equilibrium of aqua–chloro species by simply dissolving $Cp'Ru(NO)Cl_2$ in H_2O (eq 13). Conductivity, pH measurements, and

$$Cp'Ru(NO)Cl_2 \overset{H_2O}{\rightleftharpoons} [Cp'Ru(NO)(OH_2)(Cl)]^+ + Cl^- \overset{H_2O}{\rightleftharpoons} {}^1/_2[Cp'Ru(NO)(\mu\text{-}OH)]_2^{2+} + 2Cl^- + H^+ \quad (13)$$

electronic absorption data indicate that $Cp'Ru(NO)Cl_2$ is a weak electrolyte in H_2O and that a significant amount of undissociated $Cp'Ru(NO)Cl_2$ is present in solution. ^1H NMR spectroscopy measurements in H_2O show nearly equal concentrations of $Cp'Ru(NO)Cl_2$ and $[Cp'Ru(NO)(OH_2)(Cl)]^+$ with only a minor amount of the $\mathbf{4a}^{2+}$ or $\mathbf{4b}^{2+}$ ions being present. Under these conditions, the diaqua species $\mathbf{3a}^{2+}$ or $\mathbf{3b}^{2+}$ are not observed due to the relatively large amount of Cl^- present in solution.

Deuteration of the Cp′-Methyl Groups. Although we were initially surprised to see facile H/D exchange in the Cp′-methyl groups in our Ru complexes, a perusal of the literature shows that a similar phenomenon was reported over 20 years ago by Maitlis and co-workers for the $[(Cp^*M)_2(\mu\text{-}OH)_3]^+$ complexes (M = Rh, Ir).[10a] There continues to be considerable interest in this type of reactivity, especially with regard to slippage of the Cp′ ligand to an η^4-fulvene coordination mode.[10,27]

The present study offers new insight into the mechanism of reversible H/D exchange on a hydrocarbon ligand under aqueous conditions. The specificity of deuterium incorporation into only the $Cp^\dagger$-methyl groups suggests that the relative pK_a of the Cp′ protons is the important parameter in the process. Since the pK_a of the methylene protons of the $Cp^\dagger$ ligand can be expected to be higher than the pK_a of the methyl substituents, we conclude that the H/D exchange involves an H^+ or D^+ transfer. The release of H^+ can be expected to be more facile upon Cp′ slippage. In order for the Cp′ ligand to slip, ligands like O^{2-}, OH^-, or H_2O that are capable of both σ- and π-donation are required. The absence of H/D exchange when $Cp'Ru(NO)Cl_2$ is treated with D_2O/DCl (where no H_2O or OH^- ligation occurs) suggests that Cl^- ligands alone are not capable of causing the effect. In Scheme 1, we propose a tautomerization process from the unseen μ-oxo complex, where the Cp′ ligand slips to an η^4-fulvene mode. Our experience with complexes like $\mathbf{4a}^+$ shows that exchange of H^+/D^+ could easily occur at the μ-hydroxyl positions. The decomposition at pH > 11 presumably arises from OH^- attack at the coordinated NO and greatly limits our ability to fully probe this reaction. The sluggishness of H/D exchange under acidic conditions is consistent with the need for a base to accept a proton from the Cp′ ligand.

Summary. While our previous study has shown the ability of [Cp*Ru(NO)(R)(OTf)] complexes to bind and activate alkynes via OTf^- substitution,[11] the present study provides a more clear picture of the binding of OTf^- to an electrophilic metal center. We have shown that OTf^- binds quite strongly with apparent ionic and covalent interactions with the metal. In wet CH_2Cl_2, OTf^- dissociation to give aqua complexes is unfavorable due to entropy costs associated with the formation of solvated ion pairs. In neat coordinating solvents like THF, the formation of solvento complexes is much more favorable. In protic coordinating solvents like H_2O, complete OTf^- dissociation occurs due to the ease of H^+ ionization from the bound-H_2O ligand facilitated by the extremely electrophilic $[Cp'Ru(NO)]^{2+}$ moiety. The response of the NO ligand to H_2O coordination shows the H_2O ligand to be a significant π- and σ-donor. Such π-donation may possibly be a factor in the observed H/D exchange on the Cp′-ligand methyl positions and may have implications about the role of H_2O in other catalytic processes. We are continuing our studies of the ability of the $[Cp'Ru(NO)]^{2+}$ fragment to bind and activate alcohols and ethers under similar aqueous conditions.

Experimental Section

General Methods. Standard Schlenk techniques were employed in all syntheses. The nitrogen reaction atmosphere was purified by passing through scavengers for water (Aquasorb, Mallinckrodt) and oxygen (Catalyst R3-11, Chemical Dynamics, So. Plainfield, NJ). Organic solvents were distilled under nitrogen over appropriate drying agents prior to use. The water used was purified and deionized (NANO-pure Ultrapure Water System) and saturated with N_2 gas prior to use. Concentration of H_2O in water-saturated CH_2Cl_2 at 298 K is 0.198 g of H_2O/100 mL of CH_2Cl_2 (ca. 0.1 M) as taken from the literature.[28] All chemical reagents were used as received from Aldrich unless stated otherwise. Cp*Ru(NO)-Cl_2[12a] and Cp*Ru(NO)$(CH_3)_2$[29] were prepared as previously described. The preparation of $Cp^\dagger Ru(NO)Cl_2$ and $Cp^\dagger Ru(NO)$-$(CH_3)_2$ followed similar procedures using $C_5(CH_3)_4(CH_2CH_3)H$ in place of $C_5(CH_3)_5H$; their characteristics are reported below. Infrared spectra were recorded on a Mattson Polaris-Icon FT spectrometer.

The ^1H, ^2H, ^{13}C, and ^{19}F NMR spectra were recorded on a Bruker ARX-400 NMR spectrometer operating at 400 MHz (^1H), 61.42 MHz (^2H), 100.62 MHz (^{13}C), and 376.2 MHz (^{19}F). The residual solvent peak of $CDCl_3$ was used as the internal NMR standard (^1H δ 7.24; ^{13}C δ 77.0 ppm), as well as residual peak of HDO (^1H δ 4.70). Routine spectra were recorded at 298 K. ^{19}F chemical shifts were referenced externally to $CFCl_3$ (δ 0.0) or internally to 3,5-bis(trifluoromethyl)benzene (δ −63.2); a relaxation delay of 12 s was used to optimize the integration. Free OTf^- appears at δ −78.6 in CH_2Cl_2 and δ −78.0 in H_2O, regardless of the counterions present. NMR spectra in CH_2Cl_2 and H_2O were measured using solvent presaturation techniques and were shimmed and referenced

(27) Cp* conversions to the tetramethylfulvene complexes in transition metals: (a) Werner, H.; Crisp, G. T.; Jolly, P. W.; Kraus, H.-J.; Krüger, C. *Organometallics* **1983**, *2*, 1369. (b) Parkin, G.; Bercaw, J. E. *Polyhedron* **1988**, *7*, 2053. (c) Pattiasina, J. W.; Hissink, C. E.; de Boer, J. L.; Meetsma, A.; Teuben, J. H. *J. Am. Chem. Soc.* **1985**, *107*, 7758. (d) Straus, D. A.; Zhang, C.; Tilley, T. D. *J. Organomet. Chem.* **1989**, *369*, C13. (e) Einstein, F. W. B.; Jones, R. H.; Zhang, X.; Yan, X.; Nagelkerke, R.; Sutton, D. *J. Chem. Soc., Chem. Commun.* **1989**, 1424. (f) Glueck, D. S.; Bergman, R. G. *Organometallics* **1990**, *93*, 2862.

(28) Scheflan, L.; Jacobs, M. *The Handbook of Solvents*; Van Nostrand: New York, 1953; p 112.

(29) Seidler, M. D.; Bergman, R. G. *J. Am. Chem. Soc.* **1984**, *106*, 6110.

to the signals from $CDCl_3$ sealed inside a 1.5-mm capillary located concentrically inside the 5-mm NMR tube. When necessary 5-mm NMR tubes with resealable Teflon valves were used (Brunfeld Co., Bartlesville, OK). The chemical shifts reported for the complexes in CH_2Cl_2 and H_2O are identical to those in the analogous deuterated solvents.

The equilibrium and kinetic studies utilized ^{19}F and ^1H NMR spectroscopy. The temperature inside the VT-NMR probe was calibrated according to literature procedures.[30] For van't Hoff analyses, the samples were allowed to thermally equilibrate at the desired temperatures before spectra were recorded (15−120 min). The simulation of the kinetics for the equilibration of **3a** and **4a**, and the equilibration of **4a**−**c** were performed on an IBM-compatible 486 personal computer using the program KINSIM.[19] Simulations started with initial concentrations, the stoichiometry specified in the corresponding equations, and estimated values for k_f and k_r. The values of k_f and k_r were systematically varied until a satisfactory fit to the experimental data was obtained.

Potentiometric titrations were performed with an Orion Research Model 611 digital pH/millivolt meter and a glass pH electrode calibrated with standard buffer solutions at pH = 7.0 and pH = 10.0. The ca. 0.01 M NaOH solutions were standardized with KHP immediately before the measurements. The pK_a values were taken as the pH at the midpoint of the titration and were reproducible to within 0.1 pH units. Conductivity measurements were performed on YSI Model 31A conductivity bridge. Solution series were prepared prior to the measurements in the purified water (solvent conductivity $\leq 10^{-6}\ \Omega^{-1}\ cm^{-1}$) by serial dilution (concentrations range from 6.0×10^{-3} M to 1.8×10^{-4} M of Cp*Ru(NO)Cl_2 and from 1.0×10^{-3} M to 3.5×10^{-4} M of **1a)**. The saturated Cp′Ru(NO)Cl_2 solution was prepared by saturating H_2O or D_2O for 30 min at the ambient temperatures over solid Cp′Ru(NO)Cl_2 and subsequent filtering the pale green supernatant through the pipet with a cotton plug.

Mass spectra were measured with an LKB 2091 mass spectrometer using electron impact ionization and a heated direct inlet probe. Melting points were measured with a Mel-Temp device (Laboratory Devices) in open capillaries and are uncorrected. UV−visible spectra were recorded on an HP 8452A diode array spectrophotometer. Combustion analyses were performed by Atlantic Microlab, Inc., Norcross, GA.

K_{eq} Calculations for the Solvolysis of 1a. In the solvolysis of **1a** in either 0.1 M H_2O in CH_2Cl_2 or in neat THF, the concentration of the solvating ligand (H_2O or THF) is relatively large and constant. Thus, the two-step equilibria can be represented by the eqs 1 and 2, where the solvent concentration is incorporated into the K_1 and K_2 values. A representative calculation for the solvolysis of **1a** by H_2O in CH_2Cl_2 is shown below.

A starting solution that was formally 0.0106 M **1a** and 0.1 M H_2O in CH_2Cl_2 was allowed to come to equilibrium at 290 K. The species **1a**, **2a**$^+$, and free OTf^- each have a corresponding ^{19}F NMR signal intensities represented as *a*, *b*, and *c*, respectively. The sum ($a + b + c$) represents the total ^{19}F signal that can be traced back to the initial concentration of **1a**, [**1a**]$_i$, and referenced to an internal ^{19}F standard. Given that $a = 129$, $b = 21$, and $c = 31$,

$$[\mathbf{1a}] = (a/(a+b+c))([\mathbf{1a}]_i) = [129/(129+21+31)](0.0106) = 0.00755\ \text{M}$$

$$[\mathbf{2a}] = (b/(a+b+c))([\mathbf{1a}]_i)(2) = [21/(129+21+31)](0.0106)(2) = 0.00246\ \text{M}$$

$$[OTf^-] = (c/(a+b+c))([\mathbf{1a}]_i)(2) = [31/(129+31+21)](0.0106)(2) = 0.00363\ \text{M}$$

The concentration of **3a** was deduced according to the mass conservation considerations:

$$[\mathbf{1a}]_i = [\mathbf{1a}] + [\mathbf{2a}] + [\mathbf{3a}]$$

$$[\mathbf{3a}] = [\mathbf{1a}]_i - [\mathbf{1a}] - [\mathbf{2a}] = 0.0106 - 0.00755 - 0.00246 = 0.00059\ \text{M}$$

From eq 1, K_1 and K_2 are expressed:

$$K_1 = [\mathbf{2a}][OTf^-]/[\mathbf{1a}] \qquad K_2 = [\mathbf{3a}][OTf^-]/[\mathbf{2a}]$$

Substitution of the values for [**1a**], [**2a**], [OTf^-], and [**3a**] gives:

$$K_1 = [\mathbf{2a}][OTf^-]/[\mathbf{1a}] = (0.00246)(0.00363)/(0.00755) = 0.00118$$

A similar strategy was used for the calculation of K_1 and

$$K_2 = [\mathbf{3a}][OTf^-]/[\mathbf{2a}] = (0.00059)(0.00363)/(0.00246) = 0.00086$$

K_2 in neat THF (eq 3). For the case of triflate substitution by Cl^- (eq 2), the term [Cl^-] is included directly into the equilibrium expression.

Characterization of Cp†Ru(NO)Cl_2:[31] ^1H NMR ($CDCl_3$) δ 2.17 (q, 2H, $^3J_{HH} = 7.5$ Hz, η^5-$C_5Me_4CH_2CH_3$), δ 1.16 (t, 3H, $^3J_{HH} = 7.5$ Hz, η^5-$C_5Me_4CH_2CH_3$), δ 1.84 (s, 6H, (η^5-$C_5Me_4CH_2CH_3$), 1.83 (s, 6H, (η^5-$C_5Me_4CH_2CH_3$); ^1H NMR (C_6D_6) δ 1.65 (q, 2H, $^3J_{HH} = 7.5$ Hz, η^5-$C_5Me_4CH_2CH_3$), δ 0.55 (t, 3H, $^3J_{HH} = 7.8$ Hz, η^5-$C_5Me_4CH_2CH_3$), δ 1.20 (s, 6H, η^5-$C_5Me_4CH_2CH_3$), 1.19 (s, 6H, η^5-$C_5Me_4CH_2CH_3$); $^{13}C\{^1H\}$ ($CDCl_3$) δ 113.0, 111.8, 110.6 (η^5-$C_5Me_4CH_2CH_3$), δ 17.6 (η^5-$C_5Me_4CH_2CH_3$), δ 13.0 (η^5-$C_5Me_4CH_2CH_3$), δ 9.6, δ 9.4 (η^5-$C_5Me_4CH_2CH_3$); IR (KBr) ν_{NO} 1769 cm^{-1} (vs); IR (CH_2Cl_2) ν_{NO} 1793 cm^{-1} (vs); MS (EI) [M^+] *m/e* 351 (33%), [M − Cl] *m/e* 281 (11%), [M − Cl(NO)] *m/e* 285 (82%). Anal. Calcd for $C_{11}H_{17}NOCl_2Ru$ (351.3): C, 37.64; H, 4.84; N, 3.99. Found: C, 37.57; H, 4.90; N, 3.93. Mp: 223 °C.

Characterization of Cp†Ru(NO)$(CH_3)_2$: ^1H NMR ($CDCl_3$) δ 2.15 (q, 2H, $^3J_{HH} = 7.5$ Hz, η^5-$C_5Me_4CH_2CH_3$), δ 1.06 (t, 3H, $^3J_{HH} = 7.5$ Hz, η^5-$C_5Me_4CH_2CH_3$), δ 1.76 (s, 6H, (η^5-$C_5Me_4CH_2CH_3$), 1.64 (s, 6H, (η^5-$C_5Me_4CH_2CH_3$), δ 0.47 (s, 3H, Ru−CH_3); $^{13}C\{^1H\}$ ($CDCl_3$) δ 108.1, 101.5, 100.7 (η^5-$C_5Me_4CH_2CH_3$), δ 17.9 (η^5-$C_5Me_4CH_2CH_3$), δ 15.6 (η^5-$C_5Me_4CH_2CH_3$), δ 9.3, δ 9.0 (η^5-$C_5Me_4CH_2CH_3$), δ −1.6 (Ru-CH_3); IR (CH_2Cl_2) ν_{NO} 1721 cm^{-1} (vs); mp 10 °C (oil at 25 °C).

X-ray Structural Analysis. Selected crystals were mounted in X-ray capillaries and examined on a Siemens P4 Autodiffractometer equipped with an LT-2a low-temperature device and a Mo Kα source. Unit cells were determined from the centering of a minimum of 25 randomly selected reflections with $15° \leq 2\theta \leq 30°$. Data were collected using the $\theta-2\theta$ technique, and solution of the structures was performed by Patterson methods (SHELXS program available from Siemens (Madison, WI)). The structures of **1b**, **2b**, and **4b** were refined to anisotropic convergence on a VAX 3100 workstation using *F* values (SHELXTL Plus program). The structure of **3b** was refined to anisotropic convergence on F^2 values using the PC-version of SHELXl-93 program available from Sheldrick.[32] A complete listing of structure solution and refinement is available as Supporting Information.

Synthesis of Cp′Ru(NO)$(OTf)_2$ (1a,b). $HOSO_2CF_3$ (1.60 mL, 18.08 mmol, 2.16 equiv) was added dropwise to a stirred CH_2Cl_2 solution of Cp*Ru(NO)$(CH_3)_2$ (2.48 g, 8.37 mmol) in 80 mL of CH_2Cl_2. The solution color changed from deep red to purple with gas evolution. After 1 h of vigorous stirring the solution volume was reduced to ca. 10 mL and 60 mL of diethyl ether was added to precipitate the product. The nearly colorless supernatant solution was decanted away and the product dried under vacuum, giving 4.68 g (8.29 mmol, 99%)

(30) Van Geet, A. L. *Anal. Chem.* **1970**, *42*, 679.

(31) Yi, G.-B. M.S. Thesis, Utah State University, Logan, UT, 1992.

(32) SHELXL-93 is available from Siemens Analytical X-ray Instruments, 6300 Enterprise Lane, Madison, WI 53719, or directly from G. Sheldrick, Institut für Anorganische Chemie der Universität, Tammannstrasse 4, D-37077 Göttingen, Germany: gsheldr@shelx.uni-ac.gwdg.de.

of **1a** as a purple microcrystalline powder. ^{1}H NMR (CH_2Cl_2): δ 1.88 (s, Cp*). ^{13}C{^{1}H} NMR (CH_2Cl_2): δ 119.4 (q, OSO_2CF_3, J_{C-F} = 318.4 Hz); δ 113.9 (C_5Me_5); δ 10.1 (C_5Me_5). ^{19}F{^{1}H} NMR (CH_2Cl_2): δ −77.0 (s, CF_3SO_3); IR (CH_2Cl_2): ν_{NO} 1848 cm^{-1} (vs). Mp: 209−211 °C; Anal. Calcd for $C_{12}H_{15}F_6NO_7RuS_2$: C, 25.53; H, 2.68; N, 2.48. Found: C, 25.05; H, 2.75; N, 2.43.

Complex **1b** was prepared similarly starting from $Cp^\dagger Ru(NO)(CH_3)_2$. Crystals of **1b** suitable for crystallography were grown by the slow evaporation of CH_2Cl_2 solution. ^{1}H NMR (CH_2Cl_2): δ 2.23 (q, 2H, $^3J_{HH}$ = 7.7 Hz, η^5-$C_5(CH_3)_4CH_2CH_3$); δ 1.89 (s, 6H, η^5-$C_5(CH_3)_4CH_2CH_3$); δ 1.88 (s, 6H, η^5-$C_5(CH_3)_4CH_2CH_3$); δ 1.23 (t, 3H, $^3J_{HH}$ = 7.7 Hz, η^5-$C_5(CH_3)_4CH_2CH_3$). ^{13}C{^{1}H} NMR (CH_2Cl_2): δ 119.4 (q, OSO_2CF_3, J_{C-F} = 318.4 Hz); δ 115.4, 115.3, 113.5 (η^5-$C_5(CH_3)_4CH_2CH_3$); δ 18.07 (η^5-$C_5(CH_3)_4CH_2CH_3$); δ 12.37 (η^5-$C_5(CH_3)_4CH_2CH_3$). ^{19}F{^{1}H} NMR (CH_2Cl_2): δ −77.0 (s, CF_3SO_3). IR (CH_2Cl_2): ν_{NO} 1851 cm^{-1} (vs). UV−vis (CH_2Cl_2; λ_{max}, nm (ϵ, M^{-1} cm^{-1}): 378 (830); 556 (264). Mp: 145 °C. Anal. Calcd for $C_{13}H_{17}F_6BO_7RuS_2$: C, 26.99; H, 2.96; N, 2.42. Found: C, 26.59; H, 3.12; N, 2.27.

Isolation of $Cp^\dagger Ru(NO)(H_2O)_2][OTf]_2$ (3b). A 1 mL amount of water-saturated $CDCl_3$ was treated with **1b** (0.010 g, 0.017 mmol) in a 5-mm NMR tube and allowed to stand at 25 °C. Large red crystals of **3b** began to appear on the walls of the tube after 1 h. IR (Nujol): ν_{NO} 1815 cm^{-1}. Mp: 86−88 °C. Anal. Calcd for $C_{13}H_{21}NRuO_9S_2F_6$ (614.5): C, 25.40; H, 3.42; N, 2.28. Found: C, 25.47; H, 3.50; N, 2.17.

Isolation of $Cp^\dagger Ru(NO)(H_2O)(OTf)][OTf]$ (2b). A crystalline mass of dark purple **1b** was allowed to stand in the air for 48 h giving **3b** as a red crystalline mass. IR (Nujol): ν_{NO} 1830 cm^{-1}.

Preparation of $Cp'Ru(NO)(\mu\text{-}OH)]_2[OTf]_2\cdot H_2O$ (4a,b). Stirring a solution of complex **1a** (0.046 g, 0.081 mmol) in 5 mL of H_2O produced a cloudy orange solution after 18 h at 25 °C. The mixture was extracted with 4 × 15 mL portions CH_2Cl_2 until the organic fractions were colorless. The combined CH_2Cl_2 extracts were dried over anhydrous $MgSO_4$, filtered, and taken to dryness *in vacuo* to give 0.027 g (0.031 mmol, 77%) of orange crystalline **4a**. ^{1}H NMR (CH_2Cl_2): δ 1.81 (s) (15H, Cp* major isomer); δ 1.85 (s) (15H, Cp* minor isomer); δ 4.47 (s) (2H, O*H*). ^{13}C NMR ($CDCl_3$): δ 119.8 (q, OSO_2CF_3, J_{C-F} = 318.4 Hz); δ 110.2 (C_5Me_5); δ 9.02 (C_5Me_5). ^{19}F{^{1}H} NMR (CH_2Cl_2): δ −78.6. IR (KBr): ν_{NO} 1795 cm^{-1} (vs); ν_{OH} 3241 cm^{-1} (br). UV−vis (H_2O; λ_{max}, nm (ϵ, M^{-1} cm^{-1}): 326 (3400); 372 (2000). Mp: 197 °C. Anal. Calcd for $C_{22}H_{32}N_2O_{10}Ru_2S_2F_6\cdot H_2O$ (864.8): C, 30.55; H, 3.73; N, 3.24. Found: C, 30.28; H, 3.67; N, 3.17.

The salt **4b** was prepared similarly starting from **1b**. ^{1}H NMR (CH_2Cl_2): δ 4.42 (s, 2H, μ-O*H*); δ 2.16 (q, 4H, $^3J_{HH}$= 7.7 Hz, η^5-$C_5(CH_3)_4CH_2CH_3$); δ 1.81 (s, 12H, η^5-$C_5(CH_3)_4CH_2CH_3$); δ 1.80 (s, 12H, η^5-$C_5(CH_3)_4CH_2CH_3$); δ 1.14 (t, 6H, $^3J_{HH}$ = 7.7 Hz, η^5-$C_5(CH_3)_4CH_2CH_3$) [Cp† signals of minor isomer: δ 2.20 (q, 4H, $^3J_{HH}$ = 7.7 Hz, η^5-$C_5(CH_3)_4CH_2CH_3$); δ 1.86 (s, 12H, η^5-$C_5(CH_3)_4CH_2CH_3$); δ 1.85 (s, 12H, η^5-$C_5(CH_3)_4CH_2CH_3$); δ 1.17 (t, 6H, $^3J_{HH}$= 7.7 Hz, η^5-$C_5(CH_3)_4CH_2CH_3$)]. ^{13}C{^{1}H} NMR (CH_2Cl_2): δ 119.8 (q, OSO_2CF_3, J_{C-F} = 318.4 Hz); δ 113.1, 111.0, 109.8 (η^5-$C_5Me_4CH_2CH_3$); δ 16.90 (η^5-$C_5Me_4CH_2CH_3$); δ 12.65 (η^5-$C_5Me_4CH_2CH_3$); δ 9.05, 8.72 (η^5-$C_5Me_4CH_2CH_3$). ^{19}F{^{1}H} NMR (CH_2Cl_2): δ −78.6. IR (thin film): ν_{NO} 1799 cm^{-1} (vs); ν_{OH} 3180 (br). Mp: 184 °C Anal. Calcd for $C_{24}H_{36}N_2O_{10}S_2F_6Ru_2$ (892.8): C, 32.28; H, 4.06; N, 3.14. Found: C, 32.50; H, 4.12; N, 3.06.

Formation of $(C_5(CD_3)_4CH_2CH_3)Ru(NO)Cl_2$ and $(C_5(CD_3)_5)Ru(NO)Cl_2$. To a solution of 26 mg of **4b** in 3 mL of D_2O was added 0.4 mL of 0.29 M NaOD. The solution was stirred for 2 h, and then 10 μL of concentrated DCl was added to the solution. The green precipitate immediately formed was collected and dried on the vacuum line. ^{1}H NMR (CH_2Cl_2): δ 2.17 (2H, quartet), 1.18 (3H, triplet). Small residual resonances appeared at δ 1.80 as a weak complex multiplet. ^{2}H NMR (CH_2Cl_2): δ 1.82 (s), δ 1.79 (s).

An analogous procedure was employed to obtain $(C_5(CD_3)_5)Ru(NO)Cl_2$ from aqueous solution of **4a**. ^{2}H NMR (CH_2Cl_2): δ 1.81 (s).

Treatment of **4a,b** under similar conditions using NaOH instead of NaOD resulted in no intensity changes in the ^{1}H NMR spectra. Subsequent treatment of these basic solutions with aqueous HCl produced green, crystalline $Cp^*Ru(NO)Cl_2$ and $Cp^\dagger Ru(NO)Cl_2$ upon a similar workup.

Formation of $[(Cp^*)(Cp^\dagger)Ru_2(NO)_2(\mu\text{-}OH)_2][OTf]_2$ (4c) from 1a and 1b. A solution prepared from **1a** (0.006 g, 0.01 mmol) and **1b** (0.007 g, 0.01 mmol) in 10 mL of H_2O was stirred at room temperature. Periodically, aliquots of the aqueous solutions were removed, extracted into CH_2Cl_2, dried over $MgSO_4$, and filtered. The ^{1}H NMR spectrum was then measured to observe formation of **4c**.

Crossover Reaction between 4a and 4b. Method A. Compounds **4a** (1.8 mg) and **4b** (2.2 mg) were placed in 5 mL of H_2O and allowed to stir at room temperature for 10 min. The solution was extracted with 4 × 10 mL of CH_2Cl_2 until the organic fraction was colorless and the combined extracts were concentrated to ca. 10 mL. The ^{1}H NMR spectrum of the sample was then monitored to observe formation of $\mathbf{4c}^{2+}$.

Method B. A solution prepared from 0.6 mL of dichloromethane, 2.1 mg of **4a**, and 1.7 mg of **4b** was placed in a 5-mm sealed NMR tube and held at 30 °C for 2 weeks. ^{1}H NMR spectra were periodically measured at 30 °C.

Method C. Method B was repeated using H_2O-saturated CH_2Cl_2 (0.1 M H_2O/CH_2Cl_2).

Acknowledgment. The support of the National Science Foundation (Grant CHE-9215872) to J.L.H. is gratefully acknowledged. We acknowledge the NSF (Grant CHE-9002379) and the Utah State University Research Office for jointly funding the purchase of the USU X-ray diffraction and NMR (Grant CHE-9311730) facilities.

Supporting Information Available: Complete listings of the K_{eq} values for the van't Hoff analyses and conductivity data and complete listings of atomic coordinates and equivalent isotropic displacement coefficients, bond angles and distances, anisotropic thermal parameters, and H positions and U values for **1b**, **2b**, **3b**, and **4b** (22 pages). Ordering information is given on any current masthead page.

OM960257Z